Radiochim. Acta **99**, 459–476 (2011) / **DOI** 10.1524/ract.2011.1855

Relativistic electronic structure studies on the heaviest elements

By V. Pershina*

GSI Helmholtzzentrum für Schwerionenforschung GmbH, Planckstr. 1, 64291 Darmstadt, Germany

(Received December 10, 2010; accepted in revised form April 18, 2011)

Heaviest elements / Electronic structure / Relativistic effects

Summary. Spectacular developments in relativistic quantum theory and computational algorithms in the last two decades allowed for accurate predictions of properties of the heaviest elements and their experimental behaviour. The most recent works in this area of investigations are overviewed. Preference is given to those related to experimental research. The role of relativistic effects is elucidated.

1. Introduction

Conceptually, it is the atomic number Z and ground state electronic configuration of an element that define its position in the Periodic Table. Since measurements of the electronic configurations are not feasible at the moment for the heaviest elements due to their short half-lives and low production rates, information on their chemical behaviour often serves as a ground for the placement. Such information is obtained from the state of art "one-atom-at-a-time" chemical experiments [1, 2]. They are based on the principle of the chromatographic separation either in the gas phase exploiting the differences in volatility of elements and their compounds [3, 4], or in the aqueous phase assessing the differences in complex formation [5]. The main aim of these experiments is to prove whether the new elements behave similarly to their lighter homologs in the chemical groups, or whether some deviations from the trends occur due to the strongest relativistic effects on their electron shells [6].

Knowledge of many other important properties, such as stabilities of compounds (dissociation energies, D_e and force constants, k_e), geometrical configurations, ionization potentials, IP, electron affinities, EA, and other cannot currently be measured for the heaviest elements. Thus, in this area, theoretical studies become extremely important and are often the only source of useful chemical information. They are also invaluable for predicting and/or interpreting the outcome of the sophisticated and expensive experiments with single atoms. Moreover, it is only the theory that can reveal how relativistic effects influence chemical properties: only by comparing the observed behaviour with that predicted on the basis of relativistic *vs.* non-relativistic calculations, the importance and magnitude of relativistic effects can be established.

*E-mail: V.Pershina@gsi.de.

Theoretical chemical research on the heaviest elements is not less challenging than the experimental one. It should be based on the most accurate relativistic electronic structure calculations in order to reliably predict properties and experimental behaviour of new elements and their compounds. It also needs the development of special approaches that bridge calculations with quantities that cannot be so easily predicted from calculations. Due to the recent spectacular developments in the relativistic quantum theory, computational algorithms and techniques, very accurate calculations of heavy element properties are now possible. Reliable predictions of experimental behaviour of the heaviest elements and their compounds were made on this basis. These theoretical works are overviewed here, with the preference given to those related to recent experimental research. The role of relativistic effects is discussed in detail. Previous reviews on the theoretical chemistry of the heaviest elements can be found in [2, 6–12].

2. Relativistic and QED effects for the heaviest elements

The relativistic mass increase for a particle (an electron) with velocity v is

$$m = m_0 \left[(1 - (v/c)^2\right]^{-1/2} , \quad (1)$$

where m_0 is the mass at zero velocity (rest mass) and c is the speed of light. The Bohr model for a hydrogen-like species gives the following expressions for the velocity, energy and orbital radius of an electron

$$v = (2\pi e^2/nh)Z , \quad (2)$$

$$E = -(2\pi^2 e^4/n^2h^2)mZ^2 , \quad (3)$$

$$r = Ze^2/mv^2 , \quad (4)$$

where n is the principal quantum number, e is the charge of the electron, and h is Planck's constant (see, *e.g.*, [13, 14]).

With increasing Z along the Periodic Table, the m/m_0 ratio becomes larger. For H it is 1.000027. From the sixth row onwards, this radio exceeds by 10%, so that relativistic effects cannot be neglected anymore. For example, for element 114, $m/m_0 = 1.79$ and it is 1.95 for element 118. The contraction (Eq. 4) and stabilization (Eq. 3) of the hydrogen-like s and $p_{1/2}$ electrons is a direct relativistic effect and it was shown to originate from the inner K and L shell regions [15]. This effect was found to

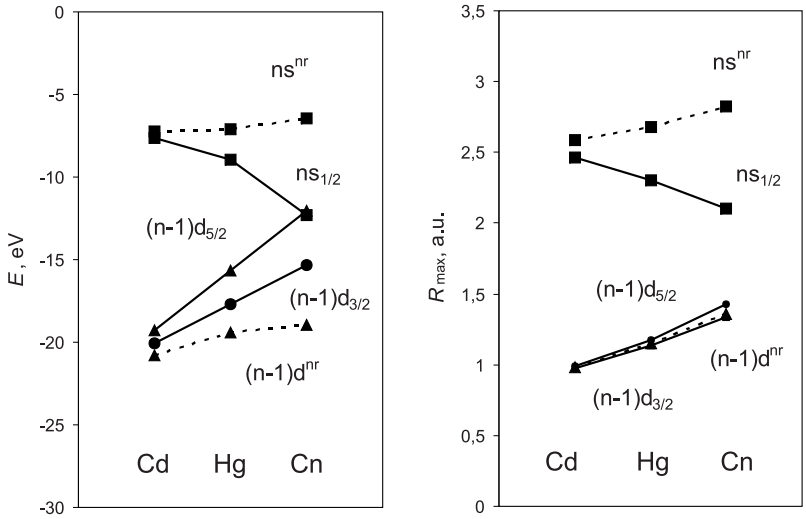

Fig. 1. Relativistic (solid line) and nonrelativistic (dashed line) energies and R_{max} of the valence ns and $(n-1)d$ AOs of the group-12 elements. The data are from [17].

be also large for the valence region due to the direct action of the relativistic perturbation operator on the inner part of the valence density [16]. As an example, Fig. 1 shows that the 7*s* atomic orbital (AO) of element 112, Cn (Copernicium), is 10 eV relativistically stabilized and 25% contracted [17].

The relativistic contraction and stabilization of the ns AO reach the maximum in the 7th row of the Periodic Table at Cn [8] (Fig. 2). The shift of the maximum to Cn in the 7th row in contrast to Au in the 6th row is due to the fact that in Rg and Cn the ground state electronic configuration is d^9s^2 and $d^{10}s^2$, respectively, while the corresponding electronic configurations in the 6th row are Au($d^{10}s^1$) and Hg($d^{10}s^2$).

The second important (indirect) relativistic effect causes an expansion and destabilization of the $p_{3/2}$, d, f and g AOs due to increased screening of the nucleus by the relativistically contracted s and $p_{1/2}$ AOs. The third important relativistic contribution comes from the spin-orbit (SO) splitting of the AOs with $l > 0$. All three effects change approximately as Z^2 for the valence shells down a column of the Periodic Table. It was suggested that relativistic effects depend even on higher powers of Z, especially for the heaviest elements [18]. Dependence of relativistic effects on electronic configuration in the neutral atoms of d- and f-block elements is discussed in [19].

The relativistic destabilization and SO splitting of the 6*d* AOs increase along the 6*d* series. Together with the stabilization of the 7*s* AOs, this results in the inversion of the 7*s* and $6d_{5/2}$ energy levels in Cn, so that its first ionized electron is $6d_{5/2}$ and not 7*s* as in Hg (Fig. 1). (An inversion of the 7*s* and $6d_{5/2}$ levels in the 7th row starts already at Hs). Fig. 1 also shows that trends in the relativistic and non-relativistic energies and R_{max} of the ns AOs (the same is valid for the $np_{1/2}$ AOs) are opposite with increasing Z in the groups, which results in the opposite trends in relativistic and nonrelativistic properties defined by those AOs.

In the 7*p* series of the elements, the stabilization of the $7s^2$ is so large that it becomes practically an inert pair. The SO splitting of the 7*p* AOs reaches 11.8 eV at element 118. For the heavier elements, relativistic effects on their valence orbitals are even more pronounced and could lead to properties that are very different to those of the lighter homologs. Without relativistic effects the properties would, however,

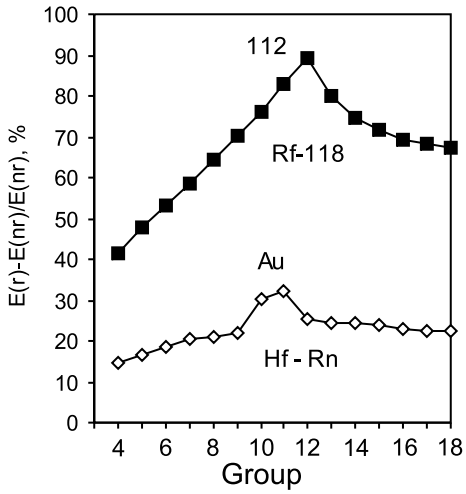

Fig. 2. The relativistic stabilization of the 6*s* and 7*s* AOs in the 6th and 7th rows of the Periodic Table. Re-drawn from [8]. The DF data are from [17].

also be very different due to the very extended diffuse valence *s*- and *p*-orbitals.

Breit effects (accounting for magnetic and retardation interactions) on valence orbital energies and IP of the heaviest elements are small, for example, only 0.02 eV for element 121 [20]. They can, however, reach a few % for the fine structure level splitting in the 7*p* elements and are of the order of correlation effects there. In element 121, they can be as large as 0.1 eV for transition energies between states including f AOs.

Quantum electrodynamic (QED) effects such as vacuum polarization and electron self-energy are known to be very important for inner-shells, for example, in accurate calculations of X-ray spectra [21, 22]. For highly charged few electron atoms they were found to be of similar size as the Breit correction to the electron–electron interaction. It was shown that the Breit and Lamb-shift terms for the valence shells behave similarly to the kinetic relativistic effects scaling as Z^2 [23]. For the group 11 and 12 valence *s*-shells, the increase in Z is even slightly larger (see Table 4 in [24]). The nuclear volume effect grows even faster with Z. Consequently, for the superheavy elements, its contribution to

the orbital energy will be the second important one after the relativistic contribution. Thus, *e.g.*, for element 118, QED effects on the binding energy of the 8s electron cause a 9% reduction (0.006 eV) of EA [25].

3. Modern quantum-chemical methods

The most appropriate quantum chemistry methods for the heaviest elements are those that treat both relativity and electron correlation at the highest level of theory. Most of them are described in [26, 27].

3.1 Atomic codes

Presently the highest theoretical level for the many-body methods is the Dirac–Coulomb–Breit (DCB) Hamiltonian

$$h_{\mathrm{DCB}} = h_{\mathrm{DC}} + \sum_{i<j} B_{ij} \,, \tag{5}$$

where the Dirac–Coulomb Hamiltonian is

$$h_{\mathrm{DC}} = \sum_{i} \left(c\boldsymbol{\alpha}_i \boldsymbol{\rho}_i + (\beta_i - 1)\right) + V^n + \sum_{i<j} 1/r_{ij} \,. \tag{6}$$

It contains the one-electron Dirac Hamiltonian plus the nuclear potential, V^n, and the operator $V_{ij} = 1/r_{ij}$ for the instantaneous Coulomb interaction between electrons. The Breit term in the low photon frequency limit is

$$B_{ij} = -1/2 \left[\left(\boldsymbol{\alpha}_i \boldsymbol{\alpha}_j\right) r_{ij}^{-1} + \left(\boldsymbol{\alpha}_i \boldsymbol{r}_{ij}\right) \left(\boldsymbol{\alpha}_j \boldsymbol{r}_{ij}\right) r_{ij}^{-3} \right] \,. \tag{7}$$

The operators of the Dirac equation (Eq. 5) are 4×4 matrix operators, and the corresponding wave function is therefore a four-component ($4c$) vector (spinor). The V^n includes the effect of the finite nuclear size, while some finer effects, like QED, can be added to h_{DCB} perturbatively, although the self-energy QED term is more difficult to treat [24]. The DCB Hamiltonian in this form (no-pair approximation) contains all effects through the second order in α, the fine-structure constant. Correlation effects are taken into account by either configuration interaction (CI), many-body perturbation theory (MBPT) or, presently at the highest level of theory, coupled cluster theory with single-double (and perturbative triple) excitations (CCSD(T)).

The Fock–Space (FS) DCB CC method [28, 29] is presently one of the most powerful methods applied for accurate atomic calculations. It currently has an accuracy of few hundredths of an eV for excitation energies in heavy elements, since it takes into account most of the dynamic electron correlation (states with high l). Many heaviest element atoms were considered within this approach. Due to the present limitation of the FS CCSD method in treating electronic configurations with no more than two electrons (holes) beyond the closed shell, calculations for the middle of the $6d$-series (elements Db through Ds) have not yet been performed. Further developments are underway to remove this limitation [29].

The DC FS CCSD method incorporated in the DIRAC program package [30] has a slightly lower accuracy than the DCB FSCC one, as Breit interactions are not yet implemented at the coupled-cluster level. The basis sets used for the elements with $Z > 103$ are typically universal ones, those of Visscher, Faegri and Dyall [31]. Prolapse-free relativistic Gaussian basis sets for elements up to $Z = 119$ suitable for $4c$ calculations have also been published [32].

A practical instrument for many-electron open-shell system is the MCDF method [33, 34]. Based on the CI technique, it accounts for most of the correlation effects while retaining a relatively small number of configurations. It omits, however, a large percentage of dynamic correlation due to limitations in the active space, which makes it less accurate than the DC(B) CCSD one. In the past, predictions of atomic properties of the heaviest elements were made with the use of the single-configuration DF and Dirac-Slater (DS) methods [6]. Atomic calculations for the heaviest elements were also performed using other approaches, like, for example, the relativistic complete active space MCSCF (CASMCSCF) CI method [35].

QED effects are presently included perturbatively in the atomic calculations on top of the SCF solutions [24, 25].

3.2 Molecular methods

Wavefunction based (ab initio) methods. The most straightforward way to solve the Dirac many-electron equation (Eq. 5) is that without approximations. Nevertheless, the problems of electron correlation and proper basis sets make the use of $4c$ *ab initio* DF methods very limited in molecular calculations. (Most of these calculations account for correlation *via* CI, Møller-Plesset, MP2, or at best, the CCSD(T) technique [36, 37]). These methods are still too computer time intensive and not sufficiently economic to be applied to the heaviest elements in a routine manner, especially to the complex systems studied experimentally. Mostly small molecules, like hydrides or fluorides, were calculated in the past. The main aim of those studies was to investigate the influence of relativistic and correlation effects on properties of model systems. One of the successful implementations of the DC method is a part of the DIRAC program package [30].

2 component (2c) methods. Due to the practical limitations of $4c$ methods, the $2c$ ones are very popular in molecular calculations. In this approximation, the "positronic" and electronic solutions of the DHF method are decoupled [38–40]. This reduces the number of matrix elements in the Hamiltonian to interactions solely among electrons (positive energy states) and nuclei and, therefore, saves valuable computer time. Perhaps the most applied method of decoupling the large and small components of the wave-function is the Douglas–Kroll–Hess approximation [41, 42].

Effective core potentials (ECP) allow for more economic calculations within the DHF schemes by replacing the inner core orbitals, which do not take part in the bond formation, by a special (effective core) potential. In this way, the number of basis functions and, therefore, two-electron integrals, is drastically diminished. There are two main types of the ECPs, pseudo potentials (PP) and model potentials (MP). For the superheavy elements, the ones available are energy-adjusted PPs [43] known as the Stuttgart ones, and the shape-consistent relativistic ECPs (RECP) [44] of Nash [45]. Generalized RECPs accounting for Breit effects were also developed for some heaviest elements [46].

As mentioned, there are also *ab initio* model potentials (AIMP) [47] that remove the drawbacks of the nodeless structure of the PPs.

Relativistic density functional theory (DFT). DFT is based on knowledge of the ground state electron density, or current, which uniquely determines the Hamiltonian, and, hence, the ground state energy and other properties of a system [48]. Due to the high accuracy and efficiency, computational schemes based on DFT methods are among the most important in theoretical chemistry, especially for extended systems, like large molecules, liquids, or solids.

For the relativistic case (see [49, 50]), the Kohn–Sham equation lying in the basis of the calculational algorithms is

$$E[\rho, j] = T_S[\rho, \boldsymbol{j}] + \int v(\boldsymbol{r})\rho(\boldsymbol{r})\,\mathrm{d}\boldsymbol{r} + \frac{1}{2}\iint \frac{\rho(\boldsymbol{r}_1)\rho(\boldsymbol{r}_2)}{|\boldsymbol{r}_1 - \boldsymbol{r}_2|}\,\mathrm{d}r_1\,\mathrm{d}r_2 - \frac{1}{2c^2}\iint \frac{\boldsymbol{j}(\boldsymbol{r}_1)\boldsymbol{j}(\boldsymbol{r}_2)}{|\boldsymbol{r}_1 - \boldsymbol{r}_2|}\,\mathrm{d}\boldsymbol{r}_1\,\mathrm{d}\boldsymbol{r}_2 + E_{xc}[\rho, \boldsymbol{j}], \quad (8)$$

where

$$\rho(\boldsymbol{r}) = \sum_i n_i \phi_i^+(\boldsymbol{r})\phi_i(\boldsymbol{r}) \quad (9)$$

is the electron density and ϕ are 4c-wave functions. $\boldsymbol{j} = (j_x, j_y, j_z)$ is the current originating from the four-current in a fully relativistic formulation, T_S is the kinetic energy and $v(\boldsymbol{r})$ is the external potential.

In principle, DFT is exact [48], but the accuracy heavily depends on the adequate choice of the exchange-correlation potential functional, E_{ex}. The exact form of the latter is, however, not known. In the past, the simplest local density approximation, LDA, was used extensively. The DS Discrete Variational (DS-DV) method [51], the predecessor of the modern relativistic DFT methods, was based on this approximation. In modern DFT methods, the generalized gradient approximation, also in the relativistic form, RGGA, is used for E_{ex} [49]. There is quite a number of GGA potentials available and their choice is dependent on the system. Thus, PBE is usually favoured by the physics community, PBE0, BLYP, B3LYP, B88/P86, *etc.* by the chemical community, while LDA is still used extensively for the solid state.

One of the most recent versions used for the heaviest element systems is the noncollinear spin-polarized (SP) 4c-DFT method [52]. According to the SP formalism, nearly each electron is treated by its own wavefunction with a quantum number j and magnetic number m_j. This permits treatment of open shell systems. The method, particularly, the embedded cluster procedure [53] (Fig. 3), allows for treatment of very large systems, which makes it suitable for study of adsorption phenomenon on surfaces of solids.

Another 4c-DFT SP method is the one developed by the Beijing group (BDF) [54]. It differs from the 4c-DFT method [52] by the basis set technique, though gives very similar results.

2c-DFT methods are a cheaper alternative to the 4c-ones [55]. Quasi-relativistic methods such as the spin-orbit zeroth-order regular approximation, SO ZORA, [56] implemented in the Amsterdam DFT code (ADF) [57] and the Douglas–Kroll–Hess (DKH) method [58] implemented in most program packages are also popular among theoretical chemists.

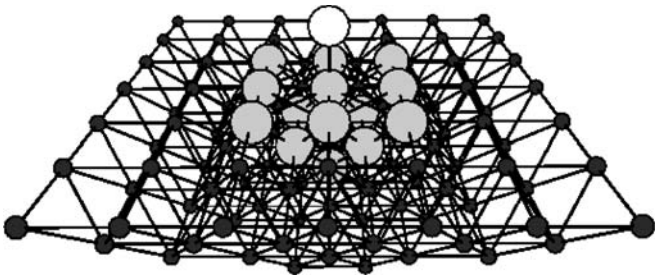

Fig. 3. Embedded M′−M$_n$ system.

4. Atomic properties

Electronic configurations. Earlier predictions of chemical properties of elements $Z = 104$ through $Z = 172$ were made on the basis of DF and DS calculations for ground states. The results are summarized in [6]. Later, DF ground states were reported for $Z = 111$ through 132 [59]. MCDF calculations for the ground and excited states of elements Rf through Hs are published in [60–64], and for ground states of elements $Z = 119$–164 in [65]. These calculations have shown that the relativistic stabilization of the 7s-AO in the 7th row results in the availability of the $7s^2$ electron pair in the ground states of the 6d and 7p elements, $7s^26d^q$ and $7s^27p^q$, respectively. This is in contrast to the 6th row, where Pt and Au have different ground states, *i.e.*, $5d^96s$ and $5d^{10}6s$, respectively.

For Rf, different MCDF calculations [60, 61] have given the $7s^27p6d$ configuration as the ground state. Presently the most accurate DCB FSCC calculations [66], however, corrected the MCDF result [59, 60] leading to the $7s^26d^2$ configuration as the ground state. A very high level of correlation with $l = 6$ was required to reach this accuracy. DC(B) FSCC calculations were also performed for elements 111–115 [67–71], 118–119 and 121–122 [25, 72–76]. They have shown that elements 119 and 120 have 8s and $8s^2$ states beyond the 118 core, respectively. Element 121 has an $8s^28p$ state in difference to Ac due to the relativistic stabilisation of the $8p_{1/2}$ AO. LDA DFT + QED calculations were reported for ground states of elements 121–131 [77].

All the calculations (except of the MCDF ones for Rf) generally agree on the ground states of the elements up to $Z = 121$. They, however, start to disagree at $Z > 121$ (see Table 1).

Elements beyond the 7th period of the Periodic Table are characterized by mixing of configurations coming from partially filled $8p_{1/2,3/2}$, $7d_{3/2,5/2}$, $6f_{5/2,7/2}$ and $5g_{7/2,9/2}$, *etc.* shells. The proximity of the valence SO bands makes the search for the correct ground state very difficult. The usual classification on the basis of a simple electronic configuration and the placement of these elements in this part of the Periodic Table becomes, therefore, problematic. Thus, *e.g.*, filling of the g shell is different in various calculations. This shell is complete at element 144 according to DF calculations [6], while it is filled at elements 143 and 145 according to DF [59] and MCDF [65] calculations, respectively.

Table 1. Ground states of element 121–124 ($Z = 120$ core +) and 143 ($Z = 120$ core + $8p_{1/2}^2$ +).

Method	121	122	123	124	⋯	143	Ref.
DF	$8p$	$7d8p$	$6f7d8p$	$6f^3 8p$		$5g^{17}6f^2 7d^2$	[6]
DF	$8p$	$7d8p$	$6f7d8p$	$6f^2 7d8p$		$5g^{18}7d^3$	[59]
MCDF	$8p$	$7d8p$	$6f^2 8p$	$6f^2 8p^2$		$5f^{17}6f^2 7d^2$	[65]
DFT	$8p$	$8p^2$	$6f7d8p$	$6f^2 8p^2$		–	[77]
DCB FSCC	$8p$	$7d8p$	–	–		–	[75, 76]

According to [6], the Periodic Table has a very long period starting from $Z = 119$ and counting 46 elements. In a recent work based on MCDF calculations of highly charged states of some elements of the 8th row, it was, however, suggested that the elements of the $5g$ series are those from $Z = 121$ to $Z = 138$ [78]. Moreover, elements 139 and 140 are assigned to group 13 and 14, respectively, so that the Periodic Table looks quite different to that of [6]. These inconsistent results indicate that starting from the 8th period, very accurate calculations with inclusion of the QED effects are required in order to reliably predict the ground states of the elements and the future shape of the Periodic Table.

Ionization potentials and electron affinities. IPs of elements 104 through 166 calculated using DF and DS methods are listed in [6]. Multiple MCDF IPs of Rf through Hs, and of Cn and element 114 are given in [62–64, 79, 80], while the first IPs of elements 113–119 are given in [81]. DCB CCSD IPs are reported for elements Rf, Rg-115, 121 and 122 [25, 66–76]. The data are summarized in [2]. According to the calculations, Cn has the largest IP in the 7th row, which is indicative of its highest chemical inertness.

IPs of internal conversion electrons ($1s$ and $2s$) for elements Mt, Cn, 114, 116 and 118 are predicted to accuracy of few eV using DHF theory and taking into account QED and nuclear-size effects [21, 22].

EAs were calculated for a few of the heaviest elements. No bound anion was found for Cn by DCB FSCC calculations [68]. Element 114 was shown to have no EA at the DC FSCC level of theory either [82]. On the contrary, element 118 has a positive EA of 0.058 eV, according to the DCB FSCC + QED calculations [25, 72], due to the relativistic stabilization of the $8s$ AO. DCB FSCC EAs of elements 119 and 121 are given in [72, 75, 83]. They are the highest in group 1 and 3, respectively.

Atomic/ionic/covalent radii and polarizabilities. Atomic radii (AR) of the heaviest elements were predicted using DS/DF calculations of R_{max} of the outer AOs [6]. Ionic radii (IR) of the group-4 through 8 elements were obtained *via* MCDF calculations of R_{max} of positively charged ions using a correlation with known IR in the chemical groups [62–64, 79, 80]. The IR were shown to be almost equal for the $4d$ and $5d$ elements, while to be about 0.5 Å larger for the $6d$ elements.

A set of atomic single and triple bond covalent radii (CR) for most of the elements of the Periodic Table including the heaviest ones till $Z = 118$ and Cn, respectively, is suggested in [84, 85]. They are deduced from the calculated molecular (equilibrium) bond lengths (R_e) of various covalent compounds. The CR of the group 4–8 $6d$ elements are also about 0.5–0.8 Å larger than those of the $5d$ elements. An important finding of these works is a decrease in the $R_{6d} - R_{5d}$ difference starting from group 9 and reaching negative values in groups 11 and 12, as a result of the relativistic bond contraction (Fig. 4). This is called a "transactinide break".

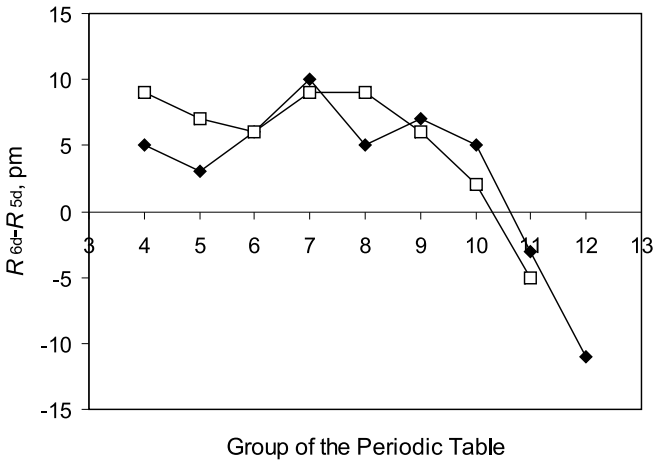

Fig. 4. The difference in the lengths of the single (filled rhomboids) and triple (open squares) bonds between the $6d$ and $5d$ metals [84, 85].

Static dipole polarizabilities, α, were calculated at the DC and KR CCSD(T) levels of theory for Cn through element 119 [83, 86–90]. A complete list of polarizabilities of the neutral elements can be found in [91]. Table 2 shows a comparison of results of various calculations for Hg and Cn. According to the calculations, α(Cn) should be the smallest in group 12 due to the relativistic contraction of the outer $7s$ AO.

Table 3 shows correlation effects on α of Pb and element 114: a decrease in Pb and an increase in element 114. Polarizabilities of elements 113 and 114 are smaller than those of In and Tl, and Sn and Pb, respectively, which is due to the

Table 2. Polarizabilities, α (in a.u.), and ionization potentials, IP (in eV), of Hg and Cn.

Method	Hg		Cn		Ref.
	α	IP	α	IP	
4c-BDF PBESIC	36.4	10.40	29.8	11.40	[92]
QR PP CCSD(T)	34.2	10.37	28.0	13.17	[92]
AR PP CCSD(T)	34.42	–	25.82	–	[93]
ECP CCSD(T)	28.48	10.39	28.68	11.675	[94]
DC CCSD(T)	34.15	–	27.64	–	[86]
DCB CCSD	–	10.445	–	11.97	[68]
exp.	33.919	10.4375	–	–	[95]

Table 3. Polarizabilities, α (in a.u.), of Pb and element 114.

Atom	Method	α				Ref.
		HF	MP2	CCSD	CCSD(T)	
Pb	DC[a]	49.91	46.75	46.98	46.96[c]	[86]
	KR[b]	49.71	47.63	47.36	47.34[d]	[90]
	exp.	–	–	–	47.1 ± 7	[90]
114	DC[a]	29.78	30.72	30.28	30.59[e]	[86]
	KR[b]	30.13	32.02	31.05	31.49[f]	[90]

a: DIRAC04 code; b: DC with Kramers symmetry in the CC procedure; c–f: the values with Gaunt contribution are: 47.7; 47.3; 31.87; 31.0, respectively.

relativistic stabilization of the $7p_{1/2}$ AO. Thus, a reversal of the trend in α is observed in groups 13 and 14 beyond In and Sn, respectively, similarly to that in AR, or $R_{max}(np_{1/2})$-AO (see Fig. 9 below).

For elements 115 through 118, α is the largest in the respective chemical groups due to the largest $R_{max}(np_{3/2})$-AO [88, 89]. Polarizability of element 118 is also the largest among the inert gases [73]. For element 119, α is relativistically decreased by 78.4 a.u., according to DK CCSD(T) calculations [83].

5. Gas-phase compounds of the 6*d*-elements

5.1 Electronic structures and properties of group-4 through 8 compounds

Electronic structures. The electronic structures of MF_4, MCl_4, MBr_4 (M = Zr, Hf and Rf), MCl_5, MBr_5, $MOCl_3$ (M = Nb, Ta and Db), MCl_6, MO_3, $MOCl_4$, MO_2Cl_2 and $M(CO)_6$ (M = Mo, W and Sg), MO_3Cl (M = Tc, Re and Bh), and MO_4 (M = Ru, Os and Hs) were studied with the use of the 4*c*-DFT method (see [7–12] for reviews). RECP calculations were also performed for some group-4 through 6 halides and oxyhalides [44, 96]. Many compounds of the type MX (M = Rf–Cn; X = H, N, B and C) and some others were also considered [84, 85].

The calculations have shown the compounds of the heaviest elements to be homologs of the lighter congeners in the chemical groups and bonding to be defined by the valence $(n-1)d$ AOs. An important finding is an increase in the stability of the maximum oxidation state and covalence in the groups, which is explained by increasing relativistic effects on the valence AOs [84, 85, 96–101]. The RECP CCSD(T) calculations for the group-6 oxyhalides [96] have shown that the SO splitting of the 6*d*-AOs is a reason for a smaller D_e of the 6*d* compounds with respect to the 5*d* ones. Importance of electron correlation accounting for about 65% of D_e (SgO_2Cl_2) was demonstrated by these calculations.

The calculations have also shown that R_e of the group-4–8 compounds of the 4*d* and 5*d* elements are almost equal as a result of the lanthanide contraction, while those of the 6*d* compounds are about 0.05–0.06 Å larger. The latter is due to both the orbital and relativistic effects on the $(n-1)d$ AOs. This is in agreement with the recent findings of CRs [84, 85] (Fig. 4).

Predictions of volatility of group-4 through 8 compounds. Prediction of ΔH_{ads} of a heavy-element molecule on a surface is presently still a formidable task for first principle calculations. A way was, therefore, suggested in [98–101] to obtain ΔH_{ads} indirectly with the use of physisorption models and accurate calculations of molecular properties. The models are based on the principle of molecule-slab interaction subdivided into usual types of long-range forces: dipole–dipole, dipole–induced dipole and van der Waals (dispersion) ones. For a symmetric molecule, *e.g.*, adsorbed on a dielectric surface, the dispersion interaction energy is [100]

$$E(x) = -\frac{3}{16}\left(\frac{\varepsilon-1}{\varepsilon+2}\right)\frac{\alpha_{mol}}{\left(\frac{1}{IP_{slab}}+\frac{1}{IP_{mol}}\right)x^3}, \qquad (10)$$

where ε is the dielectric constant of the adsorbent material. All the molecular properties of Eq. (10) can be accurately calculated using relativistic codes. The x can be deduced from the measured ΔH_{ads} for a lighter homolog in a comparative study, while x for a heavier element compound can be estimated using the difference in their AR. Similar models were developed for asymmetric molecules with dipole moments [98].

Predictions of adsorption of MO_3Cl (M = Tc, Re and Bh) on a modified (chlorinated) surface of the quartz chromatography column were made, *e.g.*, with the use of an adsorption model for molecules having non-zero dipole moments, μ [98]. Molecular properties, such as IPs, R_e, α, and μ were obtained *via* 4*c*-DFT calculations. The resulted $-\Delta H_{ads}(BhO_3Cl)$ of 78.5 kJ/mol and $-\Delta H_{ads}(TcO_3Cl)$ of 48.2 kJ/mol turned out to be in very good agreement with $-\Delta H_{ads}(BhO_3Cl)$ of 75 kJ/mol and $-\Delta H_{ads}(TcO_3Cl)$ of 51 kJ/mol measured in the isothermal gas-phase chromatography experiments [102]. The experiment has confirmed the theoretically predicted trend in volatility: $TcO_3Cl > ReO_3Cl > BhO_3Cl$. Increasing dipole moments of $MOCl_3$ in the group were shown to be responsible for this decreasing trend.

Predictions of the dispersion interaction energy of the very similar MO_4 (M = Ru, Os, and Hs) species with an inert surface (quartz) required a very high level of accuracy of the calculated molecular properties. This was achieved by using the largest possible basis sets in the 4*c*-DFT calculations [101]. The results are shown in Table 4. They are in very good agreement with experimental data for RuO_4 and OsO_4. The calculations have shown a reversal of the trend in IP and α in group 8, while R_e steadily increases (Fig. 5).

With the use of Eq. (10) one obtains $-\Delta H_{ads}(HsO_4)$ on quartz (or silicon nitride) which is larger than $-\Delta H_{ads}$ (OsO_4) (Table 4). The values indicate the same reversal of the trend in group 8 as that in α, or IP. Relativistic effects were shown to have no influence on the trends in the molecular properties and $-\Delta H_{ads}$ in group 8, since both relativistic and non-relativistic behaviour of the valence $(n-1)d$-AOs changes in the same way with increasing Z in this group.

Thermochromatography gas-phase experiments have, indeed, revealed that HsO_4 about 6 kJ/mol stronger adsorbs on inert surfaces than OsO_4 [105], with the measured

Table 4. Ionization potentials, I (in eV), polarizabilities, α (in a.u.), bond lengths, R_e (in Å), vibrational frequencies, ν_e, of the M–O bond (in cm^{-1}), molecule-surface separation distances, x (in Å), and adsorption enthalpies, $-\Delta H_{ads}$, (in kJ/mol) on quartz for MO_4 (M = Ru, Os, and Hs).

	Meth.	RuO_4	OsO_4	HsO_4	Ref.
I	Calc.	12.21	12.35	12.29	[101]
	Exp.	12.19	12.35	–	[103]
α	Calc.	58.07	55.28	65.99	[101]
	Exp.	58.64	55.13	–	[95]
R_e	Calc.	1.712	1.719	1.779	[101]
	Exp.	1.706	1.711	–	[104]
ν_e	Calc.	851	900	989	[101]
	Exp.	880	965	–	[104]
x	Calc.	2.23	2.23	2.25	[101]
$-\Delta H_{ads}$	Calc.	41.0 ± 1	39.0 ± 1	45.4 ± 1	[101]
	Exp.	–	39 ± 1	46 ± 2	[105]

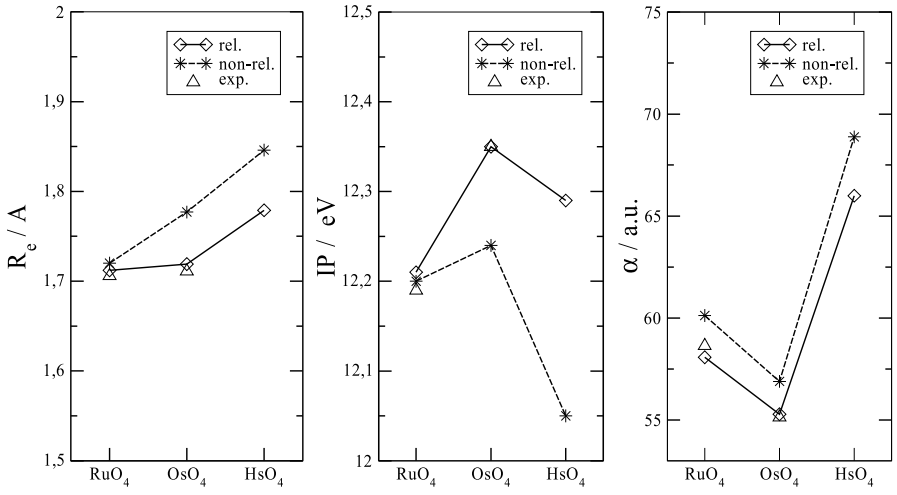

Fig. 5. Relativistic (rel.) and nonrelativistic (non-rel.) bond lengths, R_e, ionization potentials, IP, and polarizabilities, α, of MO_4 (M = Ru, Os, and Hs). From [101].

$\Delta H_{ads}(HsO_4)$ being in excellent agreement with the calculated value (Table 4).

There were some other attempts to interpret the unexpected volatility of HsO_4 [106, 107]. These works reveal, however, a deficiency of the calculations, as has clearly been demonstrated in [100].

5.2 Röntgenium

Possibility of Rg to form simple monovalent compounds and predominance of relativistic effects on its electron shells made this element an attractive object of theoretical investigations. Accordingly, a large number of calculations were performed for RgH, a sort of a test-molecule, like AuH [108, 109], using relativistic, non-relativistic, correlated, and non-correlated methods within the DC, PP and DFT formalisms [110–115]. Table 5 shows results of some calculations on R_e(RgH). One can see that the data disagree on the trend from AuH to RgH. The conclusion is, however, that R_e(RgH) should be very similar to R_e(AuH).

Large relativistic effects were found on molecular properties of RgH. The scalar relativistic effects were shown to double D_e, though the SO splitting for the Rg atom – to diminish it by 0.7 eV [114]. The trend to an increase in D_e from AgH to AuH turns, therefore, out to be inversed from AuH to RgH. The k_e of RgH should, however, be the largest of all known diatomic hydrides.

Results of various calculations [112–114] for AuX and RgX (X = F, Cl, Br, O, Au, Rg, Li) have shown that relativistic effects follow a pattern similar to that for RgH except for RgF and RgO, where the SO splitting increases D_e. The singlet state was found to be the ground one for Rg_2 in comparison with the triplet state [112]. The dissociation energy was found to change in the following order: $Au_2 > RgAu > Rg_2$.

The energies of the $MF_6^- \rightarrow MF_4^- + F_2$ and $MF_4^- \rightarrow MF_2^- + F_2$ (M = Cu, Ag, Au and Rg) decomposition reactions were calculated at the PP MP2 and CCSD levels of theory [116]. Relativistic effects were shown to stabilize higher oxidation states of Rg (*e.g.*, RgF_6^-) due to the relativistic destabilization of the 6*d* AOs and, thus, their larger involvement in the bonding. SO coupling stabilizes the molecules in the following order: $RgF_6^- > RgF_4^- > RgF_2^-$.

Table 5. Bond lengths (in Å) in AuH and RgH.

Molecule	Method	R_e	Ref.
AuH	Experiment	1.5236	[108]
RgH	DC CCSD(T)	1.522	[115]
	SO PP CCSD(T)	1.499	[114]
	PP CCSD(T)	1.529	[110]
	SC PP CCSD(T)[a]	1.506	[111]
	ADF ZORA	1.543	[84]
	DC PBE	1.558	[115]
	4*c*-BDF	1.546	[113]
	4*c*-DFT	1.520	[112]

a: shape-consistent (SC).

5.3 Copernicium

The closed-shell $6d^{10}7s^2$ ground state and predicted maximum of relativistic effects on the 7*s* AOs in group 12 and the 7th row of the Periodic Table (Fig. 2) were the reason to believe that Cn should behave like a relative inert gas. Thus, Pitzer suggested that the very high excitation energy $6d^{10}7s^2 \rightarrow 6d^{10}7s7p_{1/2}$ of 8.6 eV into the configuration of the metallic state will not be compensated by the energy gain of the metal–metal bond formation [117]. An extrapolation of ΔH_{sub} in group 12 has given 22.2 kJ/mol for Cn, which is the lowest in group 12 [118].

Experimentally, volatility of Cn in comparison with that of Hg and Rn was studied as adsorption process on a gold surface (of the chromatography column detectors) with the use of the gas-phase thermochromatography technique [119, 120]. The questions to the electronic structure theory, therefore, were: Is Cn metallic in the solid state, or is it more like a solid noble gas? How volatile and reactive towards gold is the Cn atom in comparison with Hg and Rn?

Homonuclear dimers. Bonding in the solid state of an element in the first approximation can be described by bonding in its homonuclear dimer, M_2. Knowledge of the latter was, therefore, of high importance. Moreover, Hg_2 and Cn_2 have been of particular interest for theory in checking accuracy of various methods in treating closed-shell interactions. Accordingly, the electronic structures of these dimers were calculated with the use of such methods as 4*c*-BDF, ECP

Table 6. Bond lengths, R_e (in Å), and dissociation energies, D_e (in eV), of Hg_2 and Cn_2.

Meth.	Hg_2		Cn_2		Ref.
	R_e	D_e	R_e	D_e	
4*c*-BDF PBE	3.904	0.025	3.363	0.075	[92]
QRPP CCSD(T)	3.769	0.044	3.386	0.097	[92]
4*c*-DFT B88/P86	3.63	0.01	3.45	0.05	[112]
Exp.	3.63	0.043		–	[122]

CCSD(T), QP-PP CCSD(T) [92] and 4*c*-DFT [112, 121] ones. Some results are shown in Table 6 and Fig. 6.

The calculations have shown that even though bonding both in Hg_2 and Cn_2 is preferentially of van der Waals type, a partial overlap occurs. Both the DFT and PP calculations agree on an increase in D_e of about 0.04 eV from Hg_2 to Cn_2 with the corresponding bond shortening, in line with the smaller R_{max}[7*s*(Cn) AO] in comparison with R_{max}[6*s*(Hg) AO] (Fig. 1).

Solid state. LDA DFT (non-relativistic, scalar relativistic, SR, and 4*c*-relativistic) band structure calculations on the Cn solid state [123] have shown that Cn prefers the *hcp* structure (as that of Zn and Cd) in difference to Hg (*fcc*). Thus, it should differ from its lighter homolog Hg on a structural level and resemble the solid-state noble gases. A cohesive energy, E_{coh}, of 1.13 eV was obtained for Cn at the SR level of theory, which is larger than that of Hg (0.64 eV) and is an order of magnitude larger than those of the solid noble gases. This result is consistent with the larger $D_e(Cn_2)$ with respect to $D_e(Hg_2)$ (Table 6). It was concluded that Cn is not a metal, but rather a semiconductor with a band gap of at least 0.2 eV. In this sense, Cn resembles the group-12 metals more closely than it does the noble gases.

Adsorption on inert surfaces. Adsorption of Hg and Cn on ice that can be formed in the gas-phase chromatography column below −80 °C, or on quartz used as material for the column was considered in [86, 98]. ΔH_{ads} of these elements and Rn, for a comparison purpose, were calculated using the model of Eq. (10) and DCB CCSD calculated atomic properties. It was shown that Cn should 1–2 kJ/mol stronger adsorb on these surfaces ($-\Delta H_{ads} = 26$ kJ/mol on ice and 27 kJ/mol on quartz) than Hg.

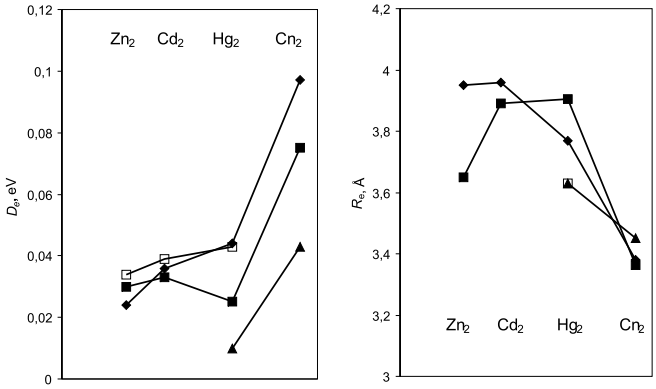

Fig. 6. QR PP CCSD(T) (filled rhomboids), 4*c*-BDF PBESIC (filled squares), 4*c*-DFT (filled triangles) and experimental (open squares) dissociation energies, D_e, and bond lengths, R_e, respectively, of the group-12 dimers (see Table 6).

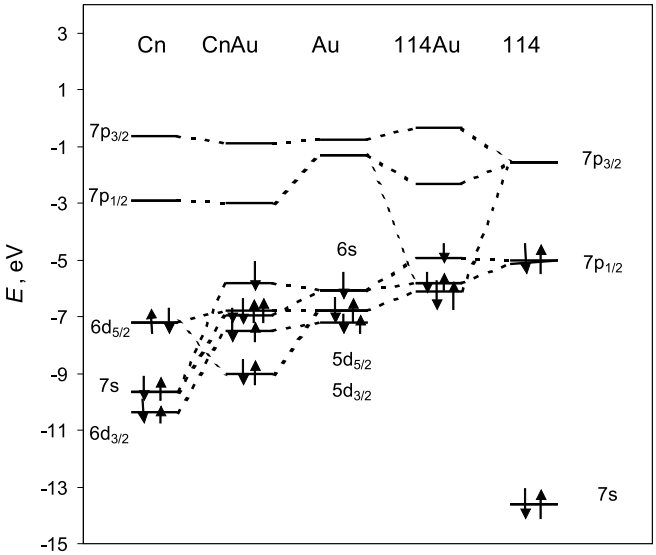

Fig. 7. Bond formation in CnAu and 114Au.

Interaction with metals. Adsorption of M = Hg and Cn on gold was predicted on the basis of the 4*c*-DFT calculations of the M–Au_n binding energies, E_b(M−Au_n), where Au_n are clusters simulating a gold surface. Such calculations usually start with the consideration of the smallest cluster, where $n = 1$. Accordingly, electronic structures of HgM and CnM, where M = Ag, Au, Pt, Pd and Cu, were calculated within the 4*c*-DFT approach [124]. It was revealed that Cn forms a chemical bond with Au primarily due to the overlap between the double occupied 7*s*(Cn) AO and single occupied 6*s*(Au) AO, as well as between the $6d_{5/2}$(Cn) and $5d_{5/2}$(Au) AOs (Fig. 7). Among M, bonding with Pd was shown to be the strongest, while with Ag the weakest.

The calculations were then extended to larger Au_n clusters [98, 125]. Since the structure of the gold layer is not known, two types of ideal surfaces, Au(100) and Au(111), were considered. In the former case, the surface was simulated by embedded Au_nAu_m clusters. The ad-atom was positioned at all possible adsorption sites: on-top, bridge and hollow. The convergence in E_b(M–Au_n) with the cluster size was reached for $n > 29$ and $m = 156$. It was found that both Cn and Hg adsorb preferentially at the bridge position, and E_b(Cn–Au_n) is 0.38 eV smaller than E_b(Hg–Au_n). With respect to the measured $-\Delta H_{ads}$(Hg) of 1.03 eV on gold [126], this gives $-\Delta H_{ads}$(Cn) = 0.67 eV. This value is in reasonably good agreement with the measured $-\Delta H_{ads}$(Cn) = $0.54^{+0.2}_{-0.01}$ eV (52^{+20}_{-4} kJ/mol) [119, 120]. The obtained absolute values of E_b of Hg and Cn are, however, larger than the measured $-\Delta H_{ads}$ of these elements on gold indicating that the Au(100) surface is not the proper one.

Next, adsorption of Cn and element 114 on the Au(111) surface was considered in [127]. The surface was modelled by Au_n clusters, where the convergence in E_b(M–Au_n) with the cluster size was reached for $n = 95$ for the top, $n = 94$ for the bridge, $n = 120$ for the hollow-1 and $n = 107$ for the hollow-2 positions. The bridge position was found again preferential for Hg, while hollow-2 for Cn. The obtained E_b(Cn–Au_n) of 0.46 eV turned out to be in good agreement with the experimental $-\Delta H_{ads}$(Cn) value [120]. The main

conclusion of both the theoretical and experimental studies is that Cn forms metal–metal bonding with gold, though weaker than Hg, and behaves like a *d*-element (and not like an inert gas) upon adsorption, thus confirming its position in group 12 of the Periodic Table.

The works on RECP and 2*c*-DFT (SO corrected) calculations for Hg and Cn interacting with small gold clusters ($n = 1$–4, and 10) [128] arrived to the same conclusion that E_b(Cn–Au$_n$) is about 0.2 eV smaller than E_b(Hg–Au$_n$). A later work of these authors based on RDFT and MBPT calculations [129] has, however given the opposite trend in the binding energies, E_b(Hg–Au$_n$) < E_b(Cn–Au$_n$), for $n = 4$ and $n = 6$. This was a reason to conclude that DFT methods are inappropriate for studying these "closed shell" systems due to deficiency in treating van der Waals interactions. The Hg/Cn–Au$_n$ are, however, chemically bound, open shell systems, where the DFT theory is totally adequate, as the results of the other calculations show [124, 125, 127]. The obtained in [129] the opposite trend in E_b of Hg and Cn might be due to inappropriate modelling of the gold clusters.

In [121], influence of relativistic effects on ΔH_{ads} of Hg and Cn on gold was investigated on the example of small M–Au$_n$ systems. Relativistic effects were shown to increase E_b(M–Au$_n$) of both Hg and Cn and to be responsible for E_b(Hg–Au$_n$) > E_b(Cn–Au$_n$).

Fig. 8 summarizes all the chemically interesting cases for group-12 elements. Thus, Cn should be stronger bound by van der Waals forces than Hg both in M_2, solid state and adsorbed state on an inert surface, and this is a relativistic effect caused by the contraction of the 7*s*(Cn) AO. The chemical M–Au bonding should decrease from Hg to Cn due to the gradual stabilization of the ns AOs. This suggests that a linear correlation between ΔH_{sub} and $-\Delta H_{ads}$, as that used in [120], is not valid in this group due to the different type of bonding in these two cases. Therefore, obtained on its basis $\Delta H_{sub}(Cn) = 38^{+10}_{-12}$ kJ/mol ($0.39^{+0.1}_{-0.12}$ eV), as well as $\Delta H_{sub}(Cn) = 22$ kJ/mol (0.23 eV) obtained *via* a straightforward extrapolation in group 12 [118] are, obviously, underestimated.

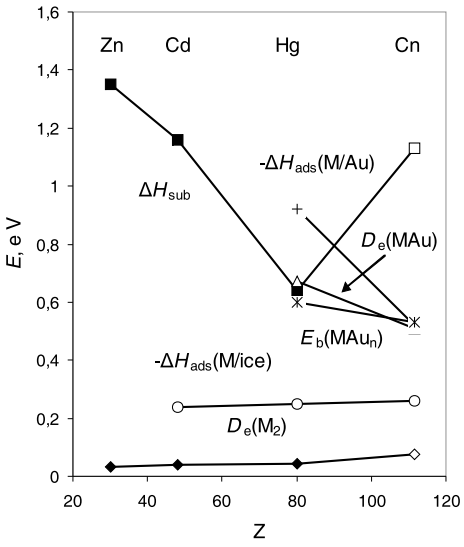

Fig. 8. Binding energies of group-12 elements in various systems: D_e of M_2 (rhomboids), $-\Delta H_{ads}$(M) on ice (circles), ΔH_{sub}(M) of metals (squares), D_e of MAu (triangles); E_b of M–Au$_n$ (stars); experimental $-\Delta H_{ads}$(M) on gold (crosses), where M = Zn, Cd, Hg and Cn. Filled symbols are experiment, open ones are calculations.

Other compounds. PP, DK2, GRECP calculations for other simple compounds of Cn, like CnH, CnH^+, CnH^- [93, 94, 115, 130, 131], demonstrated strong relativistic effect influence on their properties. Greater relativistic effects were found in $112H^+$ in comparison with RgH.

A large involvement of the 6*d* AOs of Cn in bonding in high-coordination compounds was shown by the PP CCSD(T) calculations [93]. The calculated energies of the $MF_4 \rightarrow MF_2 + F_2$ and $MF_2 \rightarrow M + F_2$ (M = Zn, Cd, Hg and Cn) decomposition reactions supported a hypothesis of increasing stability of MF_4 in the group. This was shown to be a relativistic effect.

6. 7*p* elements

Very large SO effects on the 7*p* AOs of the 7*p* elements is a reason to expect their high volatility. Early predictions based on linear extrapolations from lighter homologs in the chemical groups have, indeed, shown that elements 113 through 117 should have smaller ΔH_{sub}, or formation enthalpies of gaseous atoms, ΔH_f(g), than their lighter homologs [118].

Element 114, like Cn, was in this sense of particular interest due to the relativistic stabilization of the $7p_{1/2}$ AOs resulting in the quasi-closed shell $7s^2 7p^2_{1/2}$ ground state and, therefore, inaccessibility of these electrons for chemical bonding. The arguments of Pitzer, similar to those used for Cn, namely, that the $p^2_{1/2} \rightarrow p^2$ promotion energy to the metal valence state of element 114 will not be compensated by the metal bond formation, led to the conclusion that this element should be a relatively inert gas, or a volatile liquid bound by van der Waals forces [117].

Experimentally, volatility of element 114 was to be studied as an adsorption process on a gold surface [132, 133] with the help of the same gas-phase thermochromatograpy technique as that used for Cn [119, 120]. This should have also facilitated a direct comparison of the behaviour of these two unusual elements.

Adsorption on inert surfaces. In order to guarantee the transport of elements 113, 114 and 118 through Teflon (or PE) capillaries from the target chamber to the chemistry set up, their ΔH_{ads} on these materials were predicted *via* the physisorption model of Eq. (10) using DC(B) CCSD calculated atomic properties [73, 86, 87]. Obtained $-\Delta H_{ads}$ of 14 kJ/mol, 10.4 kJ/mol and 10.8 kJ/mol, respectively, on Teflon are relatively low, which guarantees the delivery of these elements. It was shown that the increasing trend in $-\Delta H_{ads}$ in groups 13 and 14 is reversed beyond In and Sn, respectively, with $-\Delta H_{ads}$ of elements 113 and 114 being the smallest in the corresponding groups. This reversal is caused by the decreasing atomic polarizabilities in these groups beyond In and Sn, respectively, as a result of the relativistic $np_{1/2}$ AO contraction (Fig. 9). It was also shown that element 114 should about 6 kJ/mol weaker adsorb on ice and quartz than Cn. This is due to the larger AR(114) in comparison with AR(Cn).

In group 18, $-\Delta H_{ads}$ should steadily increase with Z, with the maximum values on Rn and element 118 due to the largest α of these elements in this group [73].

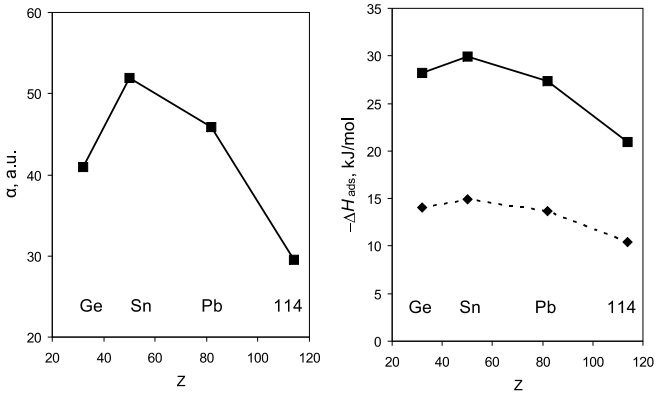

Fig. 9. DC CCSD(T) calculated polarizabilities, α, and adsorption enthalpies, $-\Delta H_{ads}$, of the group-14 elements on polyethylene (solid line) and Teflon (dashed line) [86].

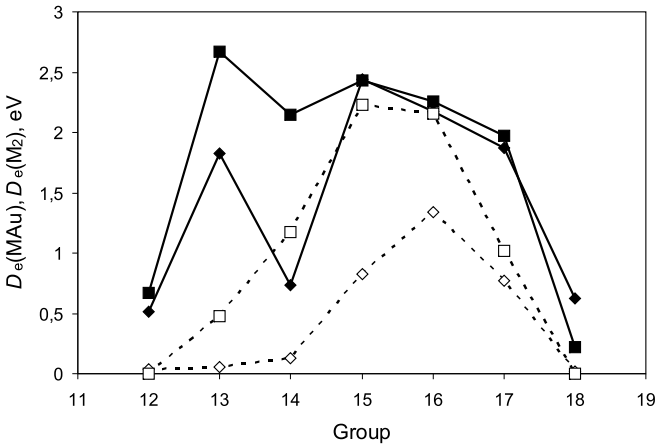

Fig. 10. Calculated dissociation energies of MAu and M_2 (M are elements Hg/Cn through Rn/118). Filled and open squares are D_e(MAu) and $D_e(M_2)$ of the $6p$ elements, respectively, while filled and open rhomboids are D_e(MAu) and $D_e(M_2)$ of the $7p$ elements, respectively [136].

Homonuclear dimers. Having in mind that bonding in M_2 is related to bonding in the solid state of M, a systematic study for the entire series of the $7p$ homonuclear dimers and their $6p$ homologs was performed using the 4*c*-DFT method [134]. The obtained $D_e(M_2)$ are shown in Fig. 10 (the dashed lines). The results for elements 113, 114, and 115 agree very well with those obtained in 4*c*-BDF, as well as 2*c*-SO ZORA calculations [55, 56, 135]. All the dimers of group-13 through 17 $7p$ elements were shown to be weaker bound than their $6p$ homologs, with the difference in $D_e(M_2)$ between them decreasing with a group number and a final reversal of the trend in group 18. The latter finding also agrees with the outcome of RECP calculations [94] (see a comparison of the results in [134]).

The maximum in $D_e(M_2)$ in the 7th row was shown to be shifted towards group 16 with respect to group 15 in the 6th and upper rows. This is a pronounced relativistic effect caused by the very large SO splitting of the $7p$ AOs. As a result of the stabilization of the $7p_{1/2}$ AOs, the system of the highest bonding-antibonding MOs in M_2 consists of only four MOs composed of the $7p_{3/2}$ AOs, so that the half-filled shell (with 4 electrons) falls on $(116)_2$. In contrast, the $6p_{1/2}$ and $6p_{3/2}$ AOs are not so well separated energetically from each other and form a set of six highest bonding-antibonding MOs, so that the half-filled shell (with 6 electrons) falls on Bi_2 (see discussions in [134]).

Table 7. Bond lengths, R_e (in Å), dissociation energies, D_e (in eV), and vibrational frequencies, ω_e (in cm^{-1}), of Pb_2 and $(114)_2$.

Molec.	Method	R_e	D_e	ω_e	Ref.
Pb_2	ECP CCSD(T)	3.06	0.64	111	[135]
	RECP CCSD(T)	2.98	0.68	–	[94]
	4*c*-BDF	2.98	1.14	108	[135]
	2*c*-DFT SO ZORA	2.97	1.16	106	[56]
	4*c*-DFT	2.97	1.18	107	[137]
	Exp.	2.93	0.86	110	[138]
	Exp.	–	1.17	–	[139]
$(114)_2$	ECP CCSD(T)	3.73	0.07	26	[135]
	4*c*-BDF	3.49	0.12	50	[135]
	2*c*-DFT SO ZORA	3.46	0.12	40	[56]
	4*c*-DFT	3.49	0.13	26	[137]

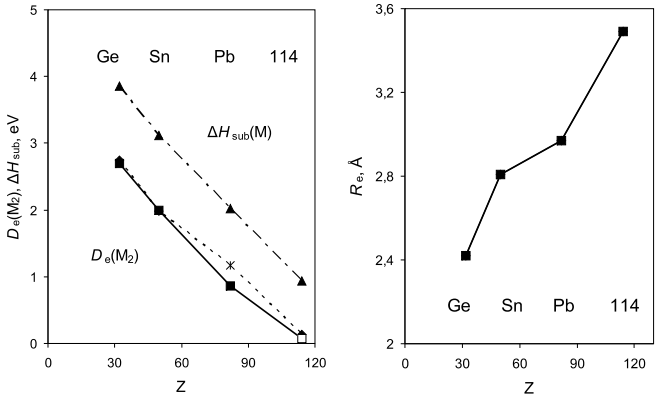

Fig. 11. Dissociation energies, $D_e(M_2)$, (experimental for Ge_2 through Pb_2: two points for Pb_2 are two different experimental values [138, 139]; and calculated for $(114)_2$: two points are two different types of calculations, 4*c*-DFT [137] and REC CCSD(T) [135]); sublimation enthalpies, ΔH_{sub}(M) [95], and calculated bond lengths, $R_e(M_2)$ [137], where M = Ge, Sn, Pb and element 114.

Element 114. A special case of $(114)_2$ as that of Cn_2 was of particular interest due to the very large stabilization and contraction of the $7p_{1/2}(114)$ AO and, therefore, expected van der Waals nature of the $7p^2_{1/2}$–$7p^2_{1/2}$ bonding. In order to test this hypothesis at the MO level of theory, the electronic structures of Pb_2 and $(114)_2$ were calculated within various approximations. Results are summarized in Table 7 and shown in Fig. 11.

All the calculations agree on the fact that $(114)_2$ is stronger bound than a typical van der Waals system. At the 4*c*-DFT level of theory, it is slightly stronger bound than Cn_2, but much weaker than Pb_2. A Mulliken population analysis indicates that both the $7p_{1/2}$ and $7p_{3/2}$ AOs of element 114 take part in the bond formation: the HOMO of σ character is composed of 98% ($7p_{1/2}$) and 2% ($7p_{3/2}$). The participation of the more extended $7p_{3/2}(114)$ AO in bonding in comparison with the $6p_{3/2}$ (Pb) AO explains an increase in R_e from Pb_2 to $(114)_2$ (Fig. 11). SO effects were shown to decrease D_e, but increase R_e in both systems [135].

Sublimation enthalpies. In [134], $\Delta H_{sub} = \Delta H_f(g)$ of the $7p$ elements were estimated *via* a correlation with the calculated $D_e(M_2)$ in the respective chemical groups. The obtained in this way $\Delta H_f(g)$ and those predicted *via* a linear

Table 8. Formation enthalpies of gaseous elements, $\Delta H_f(g)$, or sublimation enthalpies of macroamounts, ΔH_{sub} (in kJ/mol).

Method	E113	E114	E115	E116	E117
Extrapolation[a]	138.1	70.3	146.4	92.1	83.7
Correlation[b]	144.7	70.4	152 ± 12	101.3	91.7

a: Ref. [118]; b: Ref. [134].

extrapolation in the groups [118] are given in Table 8, in good agreement with each other. One can see that $\Delta H_f(g)$ changes almost linearly with Z in these groups (see Fig. 11 for group 14, as an example).

In [140], E_{coh} of element 114 was predicted from SR and SO-GGA-DFT, calculations. The obtained value of 0.5 eV (the SO-PW91 result) is in good agreement with the estimates of [134] (Table 8). SO effects were shown to lower E_{coh} and lead to structural phase transitions for the solid element 114 (the *hcp* structure in contrast to the *fcc* for Pb). In a nonrelativistic world, all group-14 elements would adopt a diamond structure [140]. An increase in the solid-state nearest-neighbour distance was found from Pb to element 114, as that in their homonuclear dimers.

Intermetallic dimers. In order to predict ΔH_{ads} of the $7p$ elements on gold, 4*c*-DFT calculations for the MAu dimers were performed in [136, 137]. Obtained D_e(MAu) in comparison with $D_e(M_2)$ are shown in Fig. 10. One can see that in groups 13 and 14, D_e(MAu) of the $7p$ elements are smaller than D_e of the $6p$ homologs (Fig. 12), in line with the trends in the energies of the $np_{1/2}$ AOs, while in groups 15 through 17, they are about the same. This is in contrast to the trends in $D_e(M_2)$ in the groups, where $D_e(Bi_2) \gg D_e[(115)_2]$, $D_e(Po_2) \gg D_e[(116)_2]$, and $D_e(At_2) > D_e[(117)_2]$. The relatively strong M−Au bonding of elements 115 through 117 with gold is explained by the relativistic destabilization of the $7p_{3/2}$ AOs fitting better to the $6s$(Au) AO, thus making – together with the $7p_{1/2}$ AO – a full σ-bond in difference to M_2, where only the $7p_{3/2}$ AOs are involved [134]. In group 18, a reversal takes place, so that $D_e(118Au) > D_e(RnAu)$, in agreement with the trend in $D_e(M_2)$. This is due to the relativistically more destabilized $7p_{3/2}(118)$ AO in comparison with the $6p_{3/2}$(Rn) AO.

The calculations have shown element 114 to be stronger bound with gold than Cn [127, 136]. This is due to the fact that in 114Au – even though both 114Au and CnAu are open shell systems with one antibonding σ^* electron–electron density is donated from the (lying higher in energy) $7p_{1/2}(114)$ AO to the $6s$(Au) AO, while in CnAu, some excitation energy is needed to transfer electron density from the closed $7s^2$(Cn) shell to the $6s$(Au) one (Fig. 7) (see [127] for a discussion).

Approximately equal D_e(MAu) of the group-15 through 17 $6p$ and $7p$ counterparts suggest that the heaviest elements should almost as strongly adsorb on gold as their lighter homologs, while element 118 – even stronger than Rn. The calculations also revealed that the M−Au bond strength *does not decrease linearly with Z* in group 15, 16 and 17. (Fig. 13 shows, *e.g.*, that in group 15, $D_e(M_2)$ and $\Delta H_f(g)$ decrease, while D_e(MAu) slightly increases with Z. Also, in group 14, a decrease in $-\Delta H_{ads}$(M) is not strictly linear with Z, see Fig. 12). No correlation between ΔH_{sub}(M) and $-\Delta H_{ads}$(M) on gold is, therefore, expected in these groups either, as well as in the 6th and 7th rows. The absence of such a correlation in the 6th row for the measured values is demonstrated in Fig. 10 of [136]. Thus, the case of the $7p$-elements with strong relativistic effects on their electron shells shows that linear extrapolations of properties such as D_e(MAu) or $-\Delta H_{ads}$(M) from the lighter homologs in the groups may be unreliable.

In [137], results of 4*c*-DFT calculations are reported for group-14 intermetallic dimers MM′, where M′ are group-10 and 11 elements Ni, Pb, Pt, Cu, Ag and Au. (Some of these metals were supposed to be used as electrode materials in electrochemical deposition experiments [5]). Bonding of element 114 with Pt was found to be the strongest, while that with Ag and Ni – the weakest. The trends in D_e and R_e of PbM′ and 114M′ as a function of M′ were shown to be determined by the trends in the energies and R_{max} of the valence $(n-1)d$ AO of the M′ atoms, respectively, and are similar for PbM′ and 114M′ (except for M′ = Ni).

Adsorption on metals. The 4*c*-DFT calculations were also performed for M = Pb and element 114, along with Hg

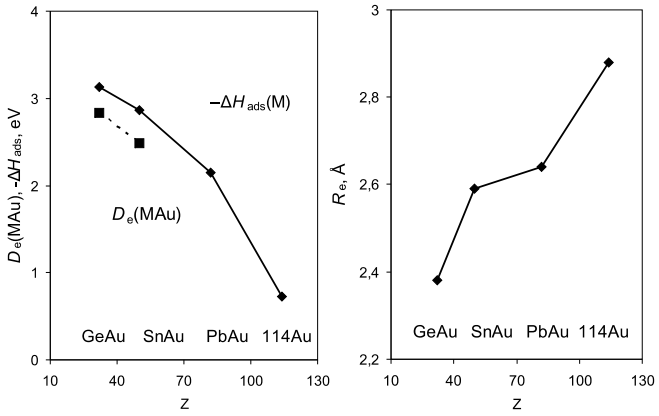

Fig. 12. Dissociation energies, D_e, (solid line – calculations [137], dashed line – experiment) and calculated bond lengths, R_e, in the MAu dimers (M = Ge, Sn, Pb and element 114). The measured $-\Delta H_{ads}$ of Pb on gold [141] is shown with an open square.

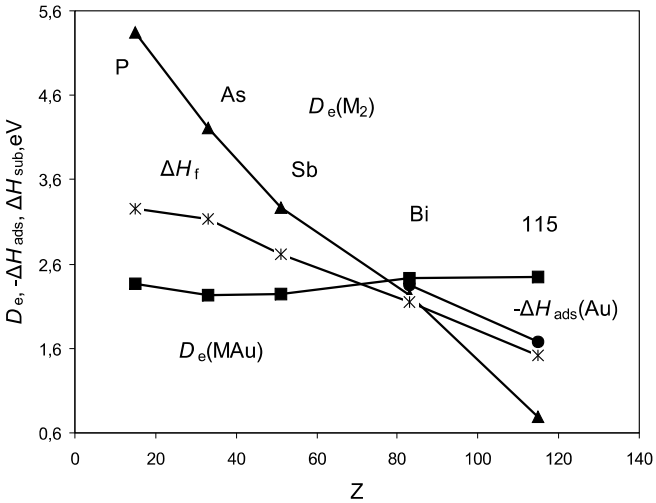

Fig. 13. Calculated dissociation energies D_e of MAu (squares) and M_2 (triangles), as well as formation enthalpies $\Delta H_f(g)$ of the group 15 elements (stars) [95, 134] and semi-empirical $-\Delta H_{ads}$ of Bi and element 115 on gold (circles) [142] (from [136]).

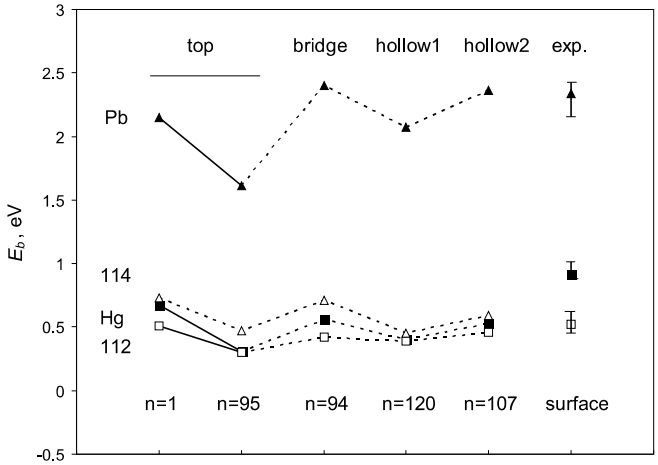

Fig. 14. 4*c*-DFT calculated binding energies of Pb, Hg, Cn and element 114 with gold clusters and experimental $-\Delta H_{ads}$ of Pb, Hg and Cn on gold (from [127]).

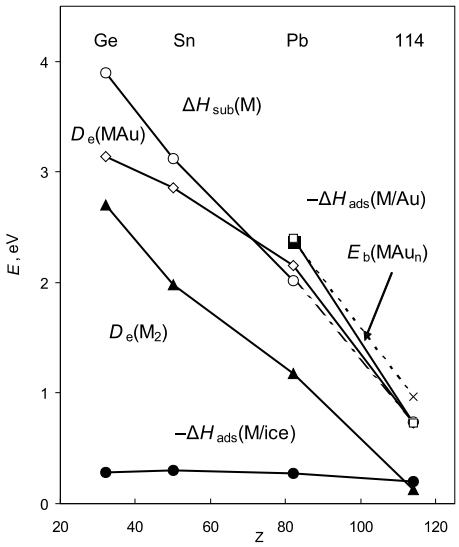

Fig. 15. Calculated dissociation energies D_e of M_2 (filled triangles [134]) and MAu (open rhomboids [136]); calculated binding energies E_b of M−Au$_n$ (open squares [127]); ΔH_{sub}, experimental for Ge, Sn and Pb, [95] and extrapolated for element 114 (open circles); experimental $-\Delta H_{ads}$(Pb) on gold (filled square) [141]; an estimated earlier $-\Delta H_{ads}$(114) (a cross) [137]; and calculated $-\Delta H_{ads}$(M) on ice (filled circles) [86].

and Cn, interacting with large Au$_n$ clusters simulating the Au(111) surface [127]. Both Pb and element 114 were found to prefer the bridge adsorption position, where the convergence in E_b(M−Au$_n$) with the cluster size was reached for $n = 94$. The calculated E_b values are in very good agreement with experimental data for Pb and Cn [120, 141] (Fig. 14) indicating that the Au(111) surface is obviously close to the real one and that element 114 forms a chemical bond with gold ($-\Delta H_{ads} = 68.5$ kJ/mol). The trend in $-\Delta H_{ads}$ for adsorption *on* the surface is predicted as Cn < Hg < 114 ≪ Pb, exactly as that obtained for the binding energies of the MAu dimers of these elements. Since Hg, as known, dissolves *into* the surface gaining another ∼ 0.3 eV, the observed trend in $-\Delta H_{ads}$ should be Cn < 114 < Hg ≪ Pb.

Calculations for the C−Au$_n$ and 114−Au$_n$ systems with the use of other relativistic DFT methods [128, 143, 144] came to the same conclusion that element 114 should form a rather strong chemical bond with gold. It should stronger adsorb on gold than Cn (Table 9).

In contradiction to the theoretical predictions, results of the first experiment on adsorption of element 114 on gold have given $-\Delta H_{ads}$ of $0.34^{+0.54}_{-0.11}$ kJ/mol with the conclusion that this value "suggests the formation of a weak physisorption bond between atomic 114 and a gold surface" [132]. For Cn, it was, however, concluded that "the stronger (than van der Waals – V.P.) adsorption interaction of element 112 with gold involves formation of a metal bond, which is

Table 9. Binding energies (in eV) of Cn−Au$_n$ and 114−Au$_n$ for the Au(100) and Au(111) surfaces.

Method	n	Cn	114	Ref.
4*c*-DFT	1	0.51	0.73	[127]
2*c*-DFT	1	0.47	0.72	[128, 144]
SO DFT	3	0.47	0.77	[128, 144]
2*c*-DFT	26^{br} Au(100)	0.33	0.55	[144]
2*c*-DFT	$37^{holl\text{-}2}$ Au(111)	–	0.49	[143]
4*c*-DFT	95^{holl} Au(111)	0.30	0.47	[127]
4*c*-DFT	94^{br} Au(111)	0.42	0.71	[127]
4*c*-DFT	$107^{holl\text{-}2}$ Au(111)	0.46	0.59	[127]
Expt.	$-\Delta H_{ads}$(M)/gold	$0.54^{+0.2}_{-0.04}$	$0.34^{+0.5}_{-0.1}$	[120, 132]

behaviour typical of group-12 elements" [119]. Thus, according to those conclusions, element 114 should be chemically more inert than Cn. The second experiment on adsorption of element 114 conducted at a lower background of interfering products registered two events of this element adsorbed on gold at the room temperature [133]. Such a relative high T_{ads} is indicative of the chemisorption process and formation of an intermetallic bond. The preliminary estimates of ΔH_{ads} support the theoretical conclusion that element 114 should be at least as reactive as Cn. Further experiments are planned to shed more light on this interesting case.

A summary of the chemical properties of group-14 elements is given in Fig. 15. For elements of this group, a decrease in all types of the interactions is observed with increasing Z, so that element 114 is the most weakly, but *chemically* bound in all types of the compounds.

To summarize a comparison of Cn and element 114. On inert surfaces, Cn should about 6 kJ/mol stronger adsorb by van der Waals forces than element 114, since R_{vdW}(Cn) < R_{vdW}(114). The M–M chemical bond in $(114)_2$ is slightly stronger than the M–M one in Cn_2, of preferentially van der Waals character, according to the DFT calculations. (However, *ab initio* DF correlated calculations for both systems would give a better ground for a direct comparison. For the solid state of Cn and element 114, a straightforward comparison of results of the different DFT calculations [123, 140] is problematic). On transition metal surfaces, element 114 should adsorb stronger than Cn, also by chemical forces, since the $7p_{1/2}$(114) AO is less stabilized than the 7*s*(Cn) AO. A comparison of properties relevant to the experimental studies on Cn and element 114 is given in Table 10.

Other compounds. Elements 113 and 114. DFC, PP, RECP, 2*c*- and 4*c*-DFT calculations were performed for MH (M = 113–118) and their lighter homologs in the chemical

Table 10. Predicted and measured properties of Cn and element 114.

Property	Cn	114
Electronic configuration	$d^{10}s^2$	$s^2p_{1/2}^2$
IP, eV	11.97	8.54
α, a.u.	27.4	29.5
AR, a.u.	3.21	3.30
R_{vdW}, a.u.	3.75	3.94
$-\Delta H_{ads}$(M)/ice, kJ/mol	26.4	20.2
$-\Delta H_{ads}$(M)/gold, kJ/mol	45	68
$-\Delta H_{ads}$(M)/gold, kJ/mol (exp.)	52^{+20}_{-4} [a]	34^{+54}_{-11} [b]

a: Ref. [120]; b: Ref. [132].

groups [112, 115, 145–150]. Influence of relativistic effects on R_e and D_e was investigated. A very large bond contraction is found in 113H due to the $7p_{1/2}$(113) AO contraction, as in none of the other compounds. D_e(114H) is diminished by relativity at most.

Formation of TlOH and 113OH was studied using the 4*c*-DFT method [151]. The 113-OH bond was found to be weaker than the Tl–OH one. Nevertheless, in the oxygen atmosphere, element 113 should form the volatile hydroxide and adsorb in this form on the gold plated detectors of the chromatography column. $-\Delta H_{ads}$(113OH) is expected to be lower that $-\Delta H_{ads}$(113) on gold.

PP, DCB, RECP and 4*c*-DFT calculations for group-13 MF have given increasing R_e and μ_e from TlF to 113F, in contrast to the decreasing values from TlH to 113H [112, 145, 146]. DF calculations for (113)(117) [152] revealed a reversal of the dipole direction and a change of the sign of the dipole moment as compared to the other group-13 homologs. PP and RECP calculations [145, 146, 148] for $113X_3$ (X = H, F, Cl, Br and I) have given the trigonal planar geometric configuration in difference to the homologs showing that the valence shell electron pair repulsion (VSERP) theory is not applicable to the heaviest elements. The stable high-coordination compound $113F_6^-$ with the metal in the 5+ oxidation state is foreseen. $113F_5$ will probably be unstable [145]. The calculated energies of the decomposition reaction $MX_3 \rightarrow MX + X_2$ (M = B, Al, Ga, In, Tl to element 113, X = H, F, Cl) suggest a decrease in the stability of the 3+ oxidation state in this group.

The electronic structures of 114X (X = F, Cl, Br, I, O, O_2) were calculated using the 2*c*-RECP CCSD(T), 2*c*-DFT SO ZORA and 4*c*-BDF methods [56, 135]. Trends in R_e and D_e for the halides and oxides from Pb to element 114 were found to be similar to those for the hydrides. In contrast to PbO_2 (D_e = 5.60 eV), $114O_2$ (D_e = 1.64 eV) was predicted to be thermodynamically unstable with respect to the decomposition into the metal atom and O_2. Using results of these calculations, it was concluded [86] that element 114 should not react with O_2 at the experimental conditions [132, 133].

Ab initio DF and PP calculations [153] for the decomposition reactions $MX_4 \rightarrow MX_2 + X_2$ and $MX_2 \rightarrow M + X_2$ (M = Si, Ge, Sn, Pb and element 114; X = H, F and Cl) predicted a decrease in the stability of the 4+ oxidation state in agreement with earlier works [6]. $114H_2$ was considered also at the CAS-MCSDF level of theory [154].

Calculations were performed for $[Pb(CO)]^{2+}$ and $[114(CO)]^{2+}$ using the DC DFT method [155]. The M–C bond lengths and complexation energies were found to be larger for the 114-complex than for the Pb one.

Elements 115 through 117. The chemistry of elements 115 and 116 has received little attention so far. It is also expected to be very interesting due to the strong SO effects on the 7*p* shell. 117H, 117F and 117Cl were considered at the DC, DFT and RECP CCSD(T) levels of theory [44, 148, 156, 157]. It was found that bonding in 117H should be weaker than in the other groups-17 MH molecules. D_e(117F) was shown to be the largest among the group-17 fluorides due to the strong SO effects. The RECP calculations have shown that the D_{3h} geometry is not the proper one for $117F_3$ in difference from At, thus indicating that the VSERP theory is not applicable to the heaviest elements [44]. An anomalous bond angle was found in $116H_2$, an evidence for the supervalent hybridization [158].

Element 118. RECP calculations for the reactions $M + F_2 \rightarrow MF_2$ and $MF_2 + F_2 \rightarrow MF_4$, where M = Xe, Rn and element 118, indicated the increasing stability of the 2+ and 4+ oxidation states in the group [44, 145]. The following trends in the stability of the fluorides were established: $RnF_2 < HgF_2 < PbF_2$, while $112F_2 < 114F_2 < 118F_2$.

Influence of the SO interaction on the geometry of $118F_4$ was investigated by RECP-SOCI and -CCSD calculations [147, 159, 160]. It was shown that a D_{4h} geometrical configuration known for XeF_4 and RnF_4 becomes about 0.2 eV less stable than the T_d one. The reason for this is availability of only stereochemically active $7p_{3/2}$ electrons for bonding. This is another example of inapplicability of the VSERP theory for the heaviest elements. An important observation was made that the fluorides of element 118 will most probably be ionic rather than covalent, as in the case of Xe. This prediction might be useful for future gas-phase chromatography experiments.

Until now, no studies were performed at the MO level for compounds of elements heavier than 118, except for PP calculations of the hydrides and fluorides of elements 119 and 120 [161], and non-correlated DF calculations for fluorides, chlorides and oxides of element 126 [162, 163].

Summary of the predictions. Predicted trends in volatility of the heaviest elements and their compounds compared to the experimental observations are summarized in Table 11. All the predictions were confirmed by experiments, except for element 114, where the final word has not yet been said. Also, the predicted values of ΔH_{ads} are in very good agreement with the experimental ones, as is shown above.

7. Complex formation and extraction by liquid chromatography

A number of theoretical works were devoted to predictions of complex formation and extraction behaviour of Rf, Db, Sg, and Hs and their group-4, 5, 6, and 8 lighter homologs from aqueous acid solutions (see [2, 9–12] for the reviews). The predictions were made with the use of a model that treats a free energy change of a complex formation reaction as a sum of the ionic and covalent contributions.

Table 11. Trends in volatility of the heaviest element compounds and their lighter homologs in the chemical groups.

Gr.	Compounds	Theoretically predicted	Ref.	Experimentally observed	Ref.
4	MCl_4, MBr_4	Hf < Rf	[164]	Hf < Rf	[168]
5	MCl_5	Nb < Ta < Db	[165]	(DbO_3Br)	[169]
	MBr_5	$DbCl_5 > DbOCl_3$	[165]	$DbCl_5 > DbOCl_3$	[169]
6	MO_2Cl_2	Mo > W > Sg	[166, 167]	Mo > W > Sg	[170, 171]
7	MO_3Cl	Tc > Re > Bh	[98]	Tc > Re > Bh	[102]
8	MO_4	Ru < Os > Hs	[101]	Os > Hs	[105]
12	M	Hg < Cn	[125, 127]	Hg < Cn	[119]
14	M	114 < Cn	[127]	114 > Cn	[132]
				114 ≤ Cn	[133]

Both are obtained *via* 4*c*-DFT electronic structure calculations [172, 173].

The results have shown that even though the heaviest elements are homologs of their lighter congeners in the chemical groups, trends in the complex formation are not necessarily continued with them. (See, *e.g.*, predictions of an unexpected trend in the distribution coefficients, K_d, of the group-5 complexes by extraction from the HCl solutions into amines [172], confirmed by experiments). The calculations have also shown that the theory of hydrolysis based on the ratio of the cation size to its charge does not explain, *e.g.*, the difference between Nb and Ta, or Mo and W [172–174]. Only by performing relativistic calculations for equilibrium reactions existing in real solutions, can complex formation, or hydrolysis constants and their order in the chemical groups be correctly predicted.

As an example, in [175] relative values of the free energy change of the $M(SO_4)_2(H_2O)_4$, $M(SO_4)_3(H_2O)_2^{2-}$ and $M(SO_4)_4^{4-}$ (M = Zr, Hf, and Rf) formation reactions from hydrated and partially hydrolyzed cations of these elements were determined using the 4*c*-DFT method.

The results indicate the following trend in the complex formation: Zr > Hf ≫ Rf. The obtained on their basis log K_d for extraction of Zr, Hf and Rf from the H_2SO_4 solutions by amines are shown in Fig. 16. Corresponding experiments confirmed the theoretical trend and have given the K_d(Rf) values close to the predicted ones [176].

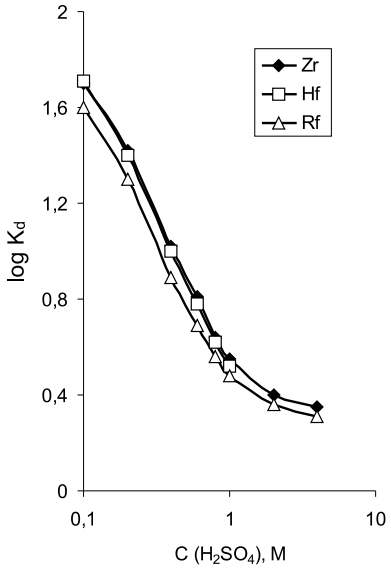

Fig. 16. Predicted log K_d values for the extraction of Hf and Rf by amines with respect to the measured one for Zr. From [175].

A summary of the predicted trends in hydrolysis, complex formation and extraction of the heaviest element complexes and their homologs as compared to experimental results is given in [2, 12]. As one can see there, most of the predictions were confirmed by the experiments carried out for the heaviest elements and their homologs, while some of them are still awaiting the confirmation, as in the case of complex formation of Sg in the HF solutions.

Redox potentials, E°, of Rf through Sg were predicted on the basis of the MCDF calculations of multiple IPs and a correlation with known E° in the chemical groups [177–179]. The E° values are given in [2]. In [180], E° for element 117 are predicted on the basis of MCDF calculations of IP and EA. The −1 state was shown to be less stable for element 117 than for At.

8. Summary and outlook

A large number of theoretical chemical studies were performed in the last two decades on the heaviest elements in the Periodic Table and their compounds. With many of them carried out in a close link to current experimental research, these studies have contributed to a better understanding of the chemistry of these exotic elements, and the role and magnitude of relativistic effects.

Atomic structures were most accurately predicted at the DCB CCFS level up to $Z = 122$. For the heavier elements, there is still some uncertainty in the ground states, so that the structure of the 8th row of the Periodic Table is still being discussed and debated.

Molecular calculations were performed for Rf through $Z = 118$ using a variety of relativistic methods, from more accurate DF *ab initio* ones to quasi–relativistic schemes. A most valuable information about properties of chemically interesting compounds (complex molecules, clusters and solid state) was obtained with the use of 4*c*- and 2*c*-DFT, as well as RECP/PP CCSD(T) methods. They proved to be complimentary both conceptually and quantitatively and their combination is the best way to investigate properties of the heaviest elements. These calculations allowed

for predicting valence states, geometries, types of stable compounds and experimental behaviour of these elements. A comparison with non-relativistic calculations allowed for revealing the role and magnitude of relativistic effects.

It was shown that elements Rf through 118 are basically homologs of their lighter congeners in the chemical groups, though their properties may be different due to the very large relativistic effects. This is also a reason why trends in atomic and molecular properties may change in moving to the heaviest elements. Thus, a straightforward extrapolation in the chemical groups may result in erroneous predictions.

Future theoretical research will very probably deal with predictions of properties of elements that have not yet been studied in detail (like Mt, or Ds) and with a more detailed study (*e.g.*, formation of new types of compounds) of the known elements. The theoretical tasks connected with predictions of experimental behaviour of elements heavier than 114 will depend on future technological developments that have to cope with very low production rates and short half-lives of these elements. In this area, theoretical chemistry will definitely have a number of exciting tasks with respect to the new objects and systems under investigation.

For elements heavier than $Z = 118$, theoretical investigations will be even more exciting, since resemblance of properties with their lighter homologues in the groups will be less pronounced. Some further methodical developments in the relativistic quantum theory, like, *e.g.*, inclusion of the QED effects on the SCF basis, may be needed to achieve a required accuracy of the predictions.

Acknowledgment. The author would like to thank J. Anton, T. Jacob, A. Borschevsky, E. Eliav and U. Kaldor for the fruitful cooperation. She also thanks A. Yakushev and C. E. Düllmann for discussions of the experimental results, as well as P. Schwerdtfeger for valuable comments on the manuscript.

References

1. Schädel, M. (ed.): *The Chemistry of the Superheavy Elements*. Dordrecht, Boston, London (2003).
2. Hoffman, D. C., Lee, D. M., Pershina, V.: Transactinide elements and future elements. In: *The Chemistry of the Actinide and Transactinide Elements*. 3rd Edn. (Morss, L. R., Edelstein, N. M., Fuger, J., eds.) Springer, Dordrecht (2006), Chapt. 14, pp. 1652–1752.
3. Gäggeler, H. W., Türler, A.: Gas-phase chemistry. In: *The Chemistry of the Superheavy Elements*. (Schädel, M., ed.) Dordrecht, Boston, London (2003), pp. 237–290.
4. Türler, A., Gregorich, K. E.: Experimental techniques. In: *The Chemistry of the Superheavy Elements*. (Schädel, M., ed.) Dordrecht, Boston, London (2003), pp. 117–158.
5. Kratz, J. V.: Liquid-phase chemistry. In: *The Chemistry of the Superheavy Elements*. (Schädel, M., ed.) Dordrecht, Boston, London (2003), pp. 159–104.
6. Fricke, B.: Struct. Bond. **21**, 89 (1975).
7. Pershina, V.: Chem. Rev. **96**, 1977 (1996).
8. Schwerdtfeger, P., Seth, M.: Relativistic effects on the superheavy elements. In: *Encyclopedia on Calculational Chemistry*. Wiley, New York (1998), Vol. 4, pp. 2480–2499.
9. Pershina, V.: Theoretical chemistry of the heaviest elements. In: *The Chemistry of the Superheavy Elements*. (Schädel, M., ed.) Dordrecht, Boston, London (2003), pp. 31–94.
10. Pershina, V.: The chemistry of the superheavy elements and relativistic effects. In: *Relativistic Electronic Structure Theory, Part II*. (Schwerdtfeger, P., ed.) Elsevier, Amsterdam (2002), pp. 1–80.
11. Pershina, V., Hoffman, D.: The chemistry of the heaviest elements. In: *Theoretical Chemistry and Physics of Heavy and Superheavy Elements*. (Kaldor, U., Wilson, S., eds.) Kluwer, Dordrecht (2003), pp. 55–114.
12. Pershina, V.: Electronic structure and chemistry of the heaviest elements. In: *Relativistic Methods for Chemists*. (Barysz, M., Ishikawa, Y., eds.) Springer, Dordrecht (2010), pp. 451–520.
13. Pyykkö, P.: Chem. Rev. **88**, 563 (1988).
14. Schwarz, W. H.: An introduction to relativistic quantum chemistry. In: *Relativistic Methods for Chemists*. (Barysz, M., Ishikawa, Y., eds.) Springer, Dordrecht (2010), pp. 1–62.
15. Schwarz, W. H. E., van Wezenbeck, E., Snijders, J. G., Baerends, E. J.: J. Phys. B **22**, 1515 (1989).
16. Baerends, E. J., Schwarz, W. H. E., Schwerdtfeger, P., Snijders, J. G.: J. Phys. B **23**, 3225 (1990).
17. Desclaux, J. P.: At. Data Nucl. Data Tab. **12**, 311 (1973).
18. Onoe, J.: Adv. Quant. Chem. **37**, 311 (2000).
19. Autschbach, J., Siekierski, S., Schwerdtfeger, P., Seth, M., Schwarz, W. H. E.: J. Comput. Chem. **23**, 804 (2002).
20. Eliav, E., Shmulyian, S., Kaldor, U., Ishikawa, Y.: J. Chem. Phys. **109**, 3954 (1998).
21. Gaston, N., Schwerdtfeger, P., Nazarewicz, W.: Phys. Rev. A **66**, 062505 (2002).
22. Thierfeld, C., Schwerdtfeger, P., Hessberger, F. P., Hofmann, S.: Eur. Phys. J. A **36**, 227 (2008).
23. Pyykkö, P., Tokman, M., Labzowsky, L. N.: Phys. Rev. A **57**, R689 (1998).
24. Thierfelder, C., Schwerdtfeger, P.: Phys. Rev. A **82**, 062503 (2010).
25. Goidenko, I., Labsowsky, L., Eliav, E., Kaldor, U., Pyykkö, P.: Phys. Rev. A **67**, 020102(R) (2003).
26. Schwerdfeger, P. (ed.): *Relativistic Electronic Structure Theory, Parts 1 and 2*. Elsevier, Amsterdam (2002).
27. Barysz, M., Ishikawa, Y. (eds.): *Relativistic Methods for Chemists*. Springer, Dordrecht (2010).
28. Eliav, E., Kaldor, U.: Four-component electronic structure methods. In: *Relativistic Methods for Chemists*. (Barysz, M., Ishikawa, Y., eds.) Springer, Dordrecht (2010), pp. 279–350.
29. Kaldor, U., Eliav, E., Landau, A.: Accurate relativistic Fock–Space calculations for many-electron atoms. In: *Relativistic Electronic Structure Theory, Parts 1 and 2*. (Schwerdfeger, P., ed.) Elsevier, Amsterdam (2002), Vol. 2, pp. 81–119.
30. DIRAC package. Dirac, a relativistic *ab initio* electronic structure program, Release DIRAC08.0 (2008), written by Jensen, H. J. A., Saue, T., Visscher, L., http://dirac.chem.sdu.dk.
31. Faegri, K., Dyall, K. G.: Basis sets for relativistic calculations. In: *Relativistic Electronic Structure Theory, Parts 1 and 2*. (Schwerdfeger, P., ed.) Elsevier, Amsterdam (2002), Part I, pp. 259–290.
32. de Macedo, L. G. M., Borin, A. C., da Silva, A. B. F.: At. Data Nucl. Data Tab. **93**, 931 (2007).
33. Desclaux, J. P.: Comp. Phys. Commun. **9**, 31 (1975).
34. Grant, I. P.: J. Phys. B **19**, 3187 (1986).
35. (a) Balasubramanian, K.: Chem. Phys. Lett. **341**, 601 (2001); (b) Balasubramanian, K.: Chem. Phys. Lett. **351**, 161 (2002).
36. Visscher, L.: Post–Dirac–Fock methods. In: *Relativistic Electronic Structure Theory, Parts 1 and 2*. (Schwerdfeger, P., ed.) Elsevier, Amsterdam (2002), Part I, pp. 291–331.
37. Saue, T.: Post Dirac–Fock–Methods-properties. In: *Relativistic Electronic Structure Theory, Parts 1 and 2*. (Schwerdfeger, P., ed.) Elsevier, Amsterdam (2002), Part I, pp. 332–400.
38. Barysz, M.: Two-component relativistic theories. In: *Relativistic Methods for Chemists*. (Barysz, M., Ishikawa, Y., eds.) Springer, Dordrecht (2010), pp. 165–190.
39. Iliaš, M., Kellö, V., Urban, M.: Acta Phys. Slovaca **60**, 259 (2010).
40. Liu, W.: Mol. Phys. **108**, 1679 (2010).
41. Douglas, M., Kroll, N. M.: Ann. Phys. **82**, 89 (1974).
42. Jansen, G., Hess, B. A.: Phys. Rev. A **39**, 6016 (1989).
43. (a) Dolg, M.: Relativistic effective core potentials. In: *Relativistic Electronic Structure Theory, Parts 1 and 2*. (Schwerdfeger, P., ed.) Elsevier, Amsterdam (2002), Part 1, pp. 793–862; (b) Cao, X., Dolg, M.: Relativistic pseudopotentials. In: *Relativistic Methods*

for Chemists. (Barysz, M., Ishikawa, Y., eds.) Springer, Dordrecht (2010), pp. 215–270.
44. Lee, Y. S.: Two-component relativistic effective core potential calculations for molecules. In: *Relativistic Electronic Structure Theory, Parts 1 and 2*. (Schwerdfeger, P., ed.) Elsevier, Amsterdam (2002), Part 2, pp. 352–416.
45. Nash, C. S., Bursten, B. E., Ermler, W. C.: J. Chem. Phys. **106**, 5153 (1997).
46. Mosyagin, N. S., Petrov, A. N., Titov, A. V., Tupitsyn, I. I.: In: *Recent Advances in the Theory of Chemical and Physical Systems*. (Julien, J.-P., ed.) Springer, Dordrecht (2006), pp. 229–251.
47. Bonifacic, V., Huzinaga, S.: J. Chem. Phys. **64**, 956 (1976).
48. Kohn, W., Becke, A. D., Parr, R. G.: J. Phys. Chem. **100**, 12974 (1996).
49. Engel, E.: Relativistic density functional theory: foundations and basic formalism. In: *Relativistic Electronic Structure Theory, Parts 1 and 2*. (Schwerdfeger, P., ed.) Elsevier, Amsterdam (2002), Part I, pp. 523–621.
50. van Wüllen, C.: Relativistic density functional theory. In: *Relativistic Methods for Chemists*. (Barysz, M., Ishikawa, Y., eds.) Springer, Dordrecht (2010), pp. 191–214.
51. (a) Rosen, A., Ellis, D. E.: J. Chem. Phys. **62**, 3039 (1975); (b) Rosen, A.: Adv. Quant. Chem. **29**, 1 (1997).
52. Anton, J., Fricke, B., Engel, E.: Phys. Rev. A **69**, 012505 (2004).
53. Jacob, T., Geschke, D., Fritzsche, S., Sepp, W.-D., Fricke, B., Anton, J., Varga, S.: Surf. Sci. **486**, 194 (2001).
54. Liu, W., Hong, G., Dai, D., Li, L., Dolg, M.: Theor. Chem. Acc. **96**, 75 (1997).
55. Mitin, A. V., van Wüllen, C.: J. Chem. Phys. **124**, 064305 (2006).
56. van Wüllen, C.: Relativistic density functional calculations on small molecules. In: *Relativistic Electronic Structure Theory, Parts 1 and 2*. (Schwerdfeger, P., ed.) Elsevier, Amsterdam (2002), Part II, pp. 598–655.
57. (a) van Lenthe, E., Ehlers, A., Baerends, E. J.: J. Chem. Phys. **110**, 8943 (1999); (b) te Velde, G., Baerends, E. J.: J. Comput. Phys. **99**, 84 (1992).
58. Hess, B. A.: Phys. Rev. A **33**, 3742 (1986).
59. Nefedov, V. I., Yarzhemcky, V. G., Trzhaskovskaya, M. B.: Russ. J. Inorg. Chem. **49**, 1871 (2004).
60. Glebov, V.A, Kasztura, L., Nefedov, V. S., Zhuikov, B. L.: Radiochim. Acta **46**, 117 (1989).
61. Johnson, E., Fricke, B., Keller Jr., O. L., Nestor Jr., C. W., Ticker, T. C.: J. Chem. Phys. **93**, 8041 (1990).
62. Fricke, B., Johnson, E., Rivery, G. M.: Radiochim. Acta **62**, 17 (1992).
63. Johnson, E., Pershina, V., Fricke, B.: J. Phys. Chem. **103**, 8458 (1999).
64. Johnson, E., Fricke, B., Jacob, T., Dong, C. Z., Fritzsche, S., Pershina, V.: J. Phys. Chem. **116**, 1862 (2002).
65. Nefedov, V. I., Trzhaskovskaya, M. B., Yarzhemcky, V. G.: Doklady Phys. Chem. **408**, 149 (2006).
66. Eliav, E., Kaldor, U., Ishikawa, Y.: Phys. Rev. Lett. **74**, 1079 (1995).
67. Eliav, E., Kaldor, U., Schwerdtfeger, P., Hess, B. A., Ishikawa, Y.: Phys. Rev. Lett. **73**, 3203 (1994).
68. Eliav, E., Kaldor, U., Ishikawa, Y.: Phys. Rev. A **52**, 2765 (1995).
69. Eliav, E., Kaldor, U., Ishikawa, Y., Seth, M., Pyykkö, P.: Phys. Rev. A **53**, 3926 (1996).
70. Landau, A., Eliav, E., Ishikawa, Y., Kaldor, U.: J. Chem. Phys. **114**, 2977 (2001).
71. Eliav, E., Kaldor, U., Ishikawa, Y.: Mol. Phys. **94**, 181 (1998).
72. Eliav, E., Kaldor, U., Ishikawa, Y., Pyykkö, P.: Phys. Rev. Lett. **77**, 5350 (1996).
73. Pershina, V., Borschevsky, A., Eliav, E., Kaldor, U.: J. Chem. Phys. **129**, 144106 (2008).
74. Landau, A., Eliav, E., Ishikava, Y., Kaldor, U.: J. Chem. Phys. **115**, 2389 (2001).
75. Eliav, E., Shmulyian, S., Kaldor, U., Ishikawa, Y.: J. Chem. Phys. **109**, 3964 (1998).
76. Eliav, E., Landau, A., Ishikawa, Y., Kaldor, U.: J. Phys. B **35**, 1693 (2002).
77. Umemoto, K., Saito, S.: J. Phys. Soc. Jap. **65**, 3175 (1996).
78. Pyykkö, P.: Phys. Chem. Chem. Phys. **13**, 161 (2011).
79. Yu, Y. J., Li, J. G., Dong, C. Z., Ding, X. B., Fritsche, S., Fricke, B.: Eur. Phys. J. D **44**, 51 (2007).
80. Yu, Y. J., Dong, C. Z., Li, J. G., Fricke, B.: J. Chem. Phys. **128**, 124316 (2008).
81. Pyper, N. C., Grant, I. P.: Proc. R. Soc. London A **376**, 483 (1981).
82. Borschevsky, A., Pershina, V., Eliav, E., Kaldor, U.: Chem. Phys. Lett. **480**, 49 (2009).
83. (a) Lim, I., Pernpointer, M., Seth, M., Schwerdtfeger, P.: Phys. Rev. A **60**, 2822 (1999); (b) Lim, I. S., Schwerdtfeger, P., Metz, B., Stoll, H.: J. Chem. Phys. **122**, 194103 (2005).
84. Pyykkö, P., Atsumi, M.: Chem. Eur. J. **15**, 186 (2009).
85. Pyykkö, P., Riedel, S., Patzsche, M.: Chem. Eur. J. **11**, 3511 (2005).
86. Pershina, V., Borschevsky, A., Eliav, E., Kaldor, U.: J. Chem. Phys. **128**, 024707 (2008).
87. Pershina, V., Borschevsky, A., Eliav, E., Kaldor, U.: J. Phys. Chem. A **112**, 13712 (2008).
88. Borschevsky, A., Pershina, V., Eliav, E., Kaldor, U.: Chem. Phys. Lett., submitted.
89. Pershina, V., Borschevsky, A.: in preparation.
90. Thierfelder, C., Assadollahzadeh, B., Schwerdtfeger, P., Schäfer, S., Schäfer, R.: Phys. Rev. A **78**, 052506 (2008).
91. Schwerdtfeger, P.: Atomic static dipole polarizabilities. In: *Computational Aspects of Electric Polarizability Calculations: Atoms, Molecules and Clusters.* (Maroulis, G., ed.) IOS Press, Amsterdam (2006), pp. 1–32. Updated static dipole polarizabilities are available as *pdf* file from the CTCP website at Massey University: http://ctcp.massey.ac.nz/dipole-polarizabilities.
92. Liu, W., Dolg, M., Schwerdtfeger, P.: unpublished.
93. Seth, M., Schwerdtfeger, P., Dolg, M.: J. Chem. Phys. **106**, 3623 (1997).
94. Nash, C. S.: J. Phys. Chem. A **109**, 3493 (2005).
95. Lide, D. R. (ed.): *CRC Handbook of Chemistry and Physics*. 86th Edn., CRC Press, Boca Raton, FL (2005).
96. Han, Y. K., Son, S.-K., Choi, Y. J., Lee, Y. S.: J. Phys. Chem. A **103**, 9109 (1999).
97. Varga, S., Fricke, B., Hirata, M., Bastug, T., Pershina, V., Fritzsche, S.: J. Phys. Chem. **104**, 6495 (2000).
98. Pershina, V., Bastug, T.: J. Chem. Phys. **113**, 1441 (2000).
99. Pershina, V., Bastug, T., Fricke, B., Varga, S.: J. Chem. Phys. **115**, 1 (2001).
100. Pershina, V., Bastug, T., Fricke, B.: J. Chem. Phys. **122**, 124301 (2005).
101. Pershina, V., Anton, J., Jacob, T.: Phys. Rev. A **78**, 032518 (2008).
102. Eichler, R., Brüchle, W., Dressler, R., Düllman, Ch. E., Eichler, B., Gäggeler, H. W., Gregorich, K. E., Hoffman, D. C., Hübener, S., Jost, D. T., Kirbach, U. W., Laue, C. A., Lavanchy, V. M., Nitsche, H., Patin, J. B., Piguet, D., Schädel, M., Shaughnessy, D. A., Strellis, D. A., Taut, S., Tobler, L., Tsyganov, Y. S., Türler, A., Vahle, A., Wilk, P. A., Yakushev, A. B.: Nature **407**, 63 (2000).
103. Burroughs, P., Evans, S., Hamnett, A., Orchard, A. F., Richardson, N. V.: J. Chem. Soc. Faraday Trans. 2 **70**, 1895 (1974).
104. (a) Krebs, B., Hasse, K. D.: Acta Crystallogr. Sect. B Struct. Crystallogr. Cryst. Chem. **32**, 1334 (1976); (b) Müller, A., Krebs, B.: J. Mol. Spectrosc. **24**, 180 (1967).
105. Düllmann, Ch. E., Brüchle, W., Dressler, R., Eberhardt, K., Eichler, B., Eichler, R., Gäggeler, H. W., Ginter, T. N., Glaus, F., Gregorich, K., Hoffman, D. C., Jäger, E., Jost, D. T., Kirbach, U. W., Lee, D. E., Nitsche, H., Patin, J. B., Pershina, V., Piguet, D., Qin, Z., Schädel, M., Schausten, B., Schimpf, E., Schött, H.-J., Soverna, S., Sudowe, R., Thörle, P., Timokhin, S. N., Trautmann, N., Türler, A., Vahle, A., Wirth, G., Yakushev, A. B., Zielinski, P. M.: Nature **418**, 859 (2002).
106. Malli, G.: J. Chem. Phys. **117**, 10441 (2002).
107. Filatov, M., Cremer, D.: J. Chem. Phys. **119**, 1412 (2003).
108. Seto, J. Y., Morbi, Z., Charron, F., Lee, S. K., Bernath, P. F., Le Roy, P. J.: J. Chem. Phys. **110**, 11756 (1999).
109. Schwerdtfeger, P., Brown, J. R., Laerdahl, J. K., Stoll, H.: J. Chem. Phys. **113**, 7110 (2000).
110. Dolg, M., Stoll, H., Seth, M., Schwerdtfeger, P.: Chem. Phys. Lett. **345**, 490 (2001).
111. Han, Y.-K., Hirao, K.: Chem. Phys. Lett. **328**, 453 (2000).

112. Anton, J., Fricke, B., Schwerdtfeger, P.: Chem. Phys. **311**, 97 (2005).
113. Liu, W., van Wüllen, Ch.: J. Chem. Phys. **110**, 3730 (1999).
114. (a) Seth, M., Schwerdtfeger, P., Dolg, M., Faegri, K., Hess, B. A., Kaldor, U.: Chem. Phys. Lett. **250**, 461 (1996); (b) Seth, M., Schwerdtfeger, P.: Chem. Phys. Lett. **318**, 314 (2000).
115. Theirfelder, C., Schwerdtfeger, P., Koers, A., Borschevsky, A., Fricke, B.: Phys. Rev. A **80**, 022501 (2009).
116. Seth, M., Cooke, F., Schwerdtfeger, P., Heully, J.-L., Pelissier, M.: J. Chem. Phys. **109**, 3935 (1998).
117. Pitzer, K. S.: J. Chem. Phys. **63**, 1032 (1975).
118. Eichler, B.: Kernenergie **10**, 307 (1976).
119. Eichler, R., Aksenov, N. V., Belozerov, A. V., Bozhikov, G. A., Chepigin, V. I., Dmitriev, S. N., Dressler, R., Gäggeler, H. W., Gorshkov, V. A., Haenssler, F., Itkis, M. G., Laube, A., Lebedev, V. Ya., Malyshev, O. N., Oganessian, Yu. Ts., Petrushkin, O. V., Piguet, D., Rasmussen, P., Shishkin, S. V., Shutov, S. V., Svirikhin, A. I., Tereshatov, E. E., Vostokin, G. K., Wegrzecki, M., Yeremin, A. V.: Nature Lett. **447**, 72 (2007).
120. Eichler, R., Aksenov, N. V., Belozerov, A. V., Bozhikov, G. A., Chepigin, V. I., Dmitriev, S. N., Dressler, R., Gäggeler, H. W., Gorshkov, A. V., Itkis, M. G., Haenssler, F., Laube, A., Lebedev, V.Ya., Malyshev, O. N., Oganessian, Y.Ts., Petrushkin, O. V., Piguet, D., Popeko, A. G., Rasmussen, P., Shishkin, S. V., Serov, A. A., Shutov, A. V., Svirikhin, A. I., Tereshatov, E. E., Vostokin, G. K., Wegrzecki, M., Yeremin, A. V.: Angew. Chem. Int Ed. **47**, 3262 (2008).
121. Pershina, V., Bastug, T.: Chem. Phys. **311**, 139 (2005).
122. Zee, R. D., Blankespoor, S. C., Zweier, T. S.: J. Chem. Phys. **88**, 4650 (1988).
123. Gaston, N., Opahle, I., Gäggeler, H. W., Schwerdtfeger, P.: Angew. Chem. Int. Ed. **46**, 1663 (2007).
124. Pershina, V., Bastug, T., Fricke, B., Jacob, T., Varga, S.: Chem. Phys. Lett. **365**, 176 (2002).
125. Sarpe-Tudoran, C., Fricke, B., Anton, J., Pershina, V.: J. Chem. Phys. **126**, 174702 (2007).
126. Soverna, S., Dressler, R., Düllmann, C. E., Eichler, B., Eichler, R., Gäggeler, H. W., Haenssler, F., Niklaus, J. P., Piguet, D., Qin, Z., Türler, A., Yakushev, A.: Radiochim. Acta **93**, 1 (2005).
127. Pershina, V., Anton, J., Jacob, T.: J. Chem. Phys. **131**, 084713 (2009).
128. (a) Rykova, E. A., Zeitsevskii, A., Mosyagin, N. S., Isaev, T. A., Titov, A. V.: J. Chem. Phys. **125**, 241102 (2006); (b) Zaitsevskii, A., Rykova, E. A., Mosyagin, N. S., Titov, A. V.: Cent. Eur. J. Phys. **4**, 448 (2006).
129. Zaitsevskii, A., van Wüllen, C., Titov, A. V.: J. Chem. Phys. **132**, 081102 (2010).
130. Mosyagin, N. S., Isaev, T. A., Titov, A. V.: J. Chem. Phys. **124**, 224302 (2006).
131. Nakajima, T., Hirao, K.: Chem. Phys. Lett. **329**, 511 (2000).
132. Eichler, R., Aksenov, N. V., Albin, Yu. V., Belozerov, A. V., Bozhikov, G. A., Chepigin, V. I., Dmitriev, S. N., Dressler, R., Gäggeler, H. W., Gorshkov, V. A., Henderson, R. A., Johnsen, A. M., Kenneally, J. M., Lebedev, V. Ya., Malyshev, O. N., Moody, K. J., Oganessian, Yu. Ts., Petrushkin, O. V., Piguet, D., Popeko, A. G., Rasmussen, P., Serov, A., Shaughnessy, D. A., Shishkin, S. V., Shutov, A. V., Stoyer, M. A., Svirikhin, A. I., Tereshatov, E. E., Vostokin, G. K., Wegrzecki, M., Wittwer, P. A., Yeremin, A. V.: Radiochim. Acta **98**, 133 (2010).
133. Yakushev, A.: private communication.
134. Pershina, V., Borschevsy, A., Anton, J., Jacob, T.: J. Chem. Phys. **132**, 194314 (2010).
135. Liu, W., van Wüllen, Ch., Han, Y. K., Choi, Y. J., Lee, Y. S.: Adv. Quant. Chem. **39**, 325 (2001).
136. Pershina, V., Borschevsy, A., Anton, J., Jacob, T.: J. Chem. Phys. **133**, 104304 (2010).
137. Pershina, V., Anton, J., Fricke, B.: J. Chem. Phys. **127**, 134310 (2007).
138. Pitzer, K. S., Balasubramanian, K.: J. Phys. Chem. **86**, 3068 (1982).
139. Heaven, M. C., Miller, T. A., Bondybey, V. E.: J. Phys. Chem. **87**, 2071 (1983).
140. Hermann, A., Furthmüller, J., Gäggeler, H. W., Schwerdtfeger, P.: Phys. Rev. B **82**, 155116 (2010).
141. (a) Haenssler, F., Eichler, R., Gäggeler, H. W., Soverna, S., Dressler, R., Piguet, D., Schippering, M.: PSI Annal Report 2004, p. 3; (b) Eichler, R.: private communication.
142. Rossbach, H., Eichler, B.: Akademie der Wissenschaft der DDR, Report No. ZFK-527 (1984).
143. Zaitsevski, A., van Wüllen, C., Rykova, E. A.: Phys. Chem. Chem. Phys. **12**, 4152 (2010).
144. Zaitsevkii, A., Titov, A.: Russ. Chem. Rev. **78**, 1173 (2009).
145. Seth, M., Schwerdtfeger, P., Faegri, K.: J. Chem. Phys. **111**, 6422 (1999).
146. Han, Y. K., Lee, Y. S.: J. Phys. Chem. A **103**, 1104 (1999).
147. Han, Y.-K., Bae, C., Son, S.-K., Lee, Y. S.: J. Chem. Phys. **112**, 2684 (2000).
148. Choi, Y. J., Han, Y. K., Lee, Y. S.: J. Chem. Phys. **115**, 3448 (2001).
149. Nash, C. S., Bursten, B. E.: J. Phys. Chem. A **103**, 632 (1999).
150. Liu, W., van Wüllen, C., Wang, F., Li, L.: J. Chem. Phys. **116**, 3626 (2002).
151. Pershina, V., Anton, J., Jacob, T.: Chem. Phys. Lett. **480**, 157 (2009).
152. Faegri, K., Saue, T.: J. Chem. Phys. **115**, 2456 (2001).
153. (a) Seth, M., Faegri, K., Schwerdtfeger, P.: Angew. Chem. Int. Ed. Engl. **37**, 2493 (1998); (b) Schwerdtfeger, P., Seth, M.: J. Nucl. Radiochem. Sci. **3**, 133 (2002).
154. Balasubramanian, K.: J. Chem. Phys. **117**, 7426 (2002).
155. Gourlaouen, C., Parisel, O., Piquemal, J.-P.: Chem. Phys. Lett. **469**, 38 (2009).
156. Visscher, L., Dyall, K. G.: J. Chem. Phys. **104**, 9040 (1996).
157. Saue, T., Faegri, K., Gropen, O.: Chem. Phys. Lett. **263**, 360 (1996).
158. Nash, C. S., Crockett, W. W.: J. Phys. Chem. A **110**, 4619 (2006).
159. Nash, C. S., Bursten, B. E.: J. Phys. Chem. A **103**, 402 (1999).
160. Nash, C. S., Bursten, B. E.: Angew. Chem. Int. Ed. **38**, 151 (1999).
161. Schwerdtfeger, P.: In: *Strength from Weakness: Structural Consequences of Weak Interactions in Molecules, Supermolecules, and Crystals*. (Domenicano, A., Hargittai, I., eds.) NATO Science Series, Kluwer, Dordrecht (2002), pp. 169–190.
162. Malli, G. L.: J. Chem. Phys. **124**, 071102 (2006).
163. Malli, G. L.: Theor. Chem. Acc. **118**, 473 (2007).
164. Pershina, V., Fricke, B.: Electronic structure and chemistry of the heaviest elements. In: *Heavy Elements and Related Phenomenon*. (Greiner, W., Gupta, Raj, K., eds.) World Scientific, Singapore (1999), Vol. I, pp. 194–262.
165. Pershina, V., Sepp, W.-D., Bastug, T., Fricke, B., Ionova, G. V.: J. Chem. Phys. **97**, 1123 (1992).
166. Pershina, V., Fricke, B.: J. Phys. Chem. **99**, 144 (1995).
167. Pershina, V., Fricke, B.: J. Phys. Chem. **100**, 8748 (1996).
168. Kadkhodayan, B., Türler, A., Gregorich, K. E., Baisden, P. A., Czerwinski, K. R., Eichler, B., Gäggeler, H. W., Hamilton, T. M., Jost, D. T., Kacher, C. D., Kovacs, A., Kreek, S. A., Lane, M. R., Mohar, M. F., Neu, M. P., Stoyer, N. J., Sylwester, E. R., Lee, D. M., Nurmia, M. J., Seaborg, G. T., Hoffman, D. C.: Radiochim. Acta **72**, 169 (1996).
169. Türler, A.: Radiochim. Acta **72**, 7 (1996).
170. Schädel, M., Brüchle, W., Dressler, R., Eichler, B., Gäggeler, H. W., Günther, R., Gregorich, K. E., Hoffman, D. C., Hübener, S., Jost, D. T., Kratz, J. V., Paulus, W., Schumann, D., Timokhin, S., Trautmann, N., Türler, A., Wirth, G., Yakushev, A. B.: Nature (Lett.) **388**, 55 (1997).
171. Türler, A., Brüchle, W., Dressler, R., Eichler, B., Eichler, R., Gäggeler, H. W., Gärtner, M., Glatz, J.-P., Gregorich, K. E., Hübener, S., Jost, D., Lebedev, T.Ya., Pershina, V., Schädel, M., Taut, S., Timokhin, N., Trautmann, N., Vahle, A., Yakushev, A. B.: Angew. Chem. Int. Ed. **38**, 2212 (1999).
172. (a) Pershina, V.: Radiochim. Acta **80**, 65 (1998); (b) Pershina, V.: Radiochim. Acta **80**, 75 (1998).
173. Pershina, V., Kratz, J. V.: Inorg. Chem. **40**, 776 (2001).
174. Pershina, V.: Radiochim. Acta **92**, 455 (2004).
175. Pershina, V., Polakova, D., Omtvedt, J. P.: Radiochim. Acta **94**, 407 (2006).
176. Omtwedt, J. P., Polyakova, D., Alstad, J., Bjornstad, T., Düllmann, C. E., Folden III, C. M., Garcia, M. A., Gates, J., Gregorich, K. E., Hoffman, D. C., Nelson, S. L., Nitsche, H., Omtwedt, L., Per-

shina, V., Samadani, F., Skarnemark, G., Stavsetra, L., Sudove, R., Wilson, R. E., Zheng, L., Zielinski, P. M.: Radiochim. Acta, to be submitted (2011).
177. Ionova, G. V., Pershina, V., Johnson, E., Fricke, B., Schädel, M.: J. Phys. Chem. **96**, 11096 (1992).
178. Pershina, V., Fricke, B.: J. Phys. Chem. **98**, 6468 (1994).
179. Pershina, V., Johnson, E., Fricke, B.: J. Phys. Chem. A **103**, 8463 (1999).
180. Chang, Z. W., Dong, C. Z., Li, J. G., Pershina, V.: in preparation (2011).